THE UNIVERSITY OF WESTERN AUSTRALIA

DEPARTMENT OF MECHANICAL & MATERIALS ENGINEERING

INFLUENCE OF TENSILE OVERLOAD ON CRACK GROWTH IN 316L STAINLESS STEEL - INCLUDING HIGH STRAIN & LOW STRESS INTERACTIONS IN 316L STAINLESS STEEL, MILD STEEL AND ALUMINIUM ALLOY 6060-T5.

H. GREGORY WHEATLEY, BE (MECH)(HONS)

SUPERVISED BY:

PROFESSOR YURI ESTRIN & A/PROFESSOR XIAO-ZHI HU

THIS THESIS IS PRESENTED FOR THE DEGREE OF

DOCTOR OF PHILOSOPHY

2001

Abstract

The fatigue crack growth behaviour of 316L stainless steel (Batch A) following a tensile overload has been observed. Micrographs and compliance measurements have also been taken. Results indicated that strain hardening may be the primary contributor toward retardation of crack growth. High strain – low stress interactions were observed in 316L stainless steel (Batch B and C), mild steel (C1020 and AS1214) and aluminium alloy (6060-T5). This was done as plasticity-induced crack closure is largely removed by using tensile specimens. Pre-training of 316L (Batch B) by low cycle fatigue (LCF) showed an increase in the fatigue life while pre-training of 316L (Batch C) showed a retardation of fatigue crack initiation and growth. Pre-training of the other materials showed little effect or a decrease in the fatigue life.

The conclusions of this thesis are as follows:

1. Fatigue crack growth occurs by a process of damage accumulation in the material in front of the crack tip.

2 Tensile overload creates a plastic deformation zone ahead of the crack tip. The material within this zone is strain hardened and also causes plasticity-induced crack closure (PICC). It has been found that retardation of post-overload fatigue crack growth is mainly a result of the increased fatigue resistance of the strain-hardened material within the overload plastic zone.

3. A tensile overload enhances the fatigue damage ahead of the crack tip. This results in a transient acceleration in the fatigue crack growth following overload.

4. 316L Stainless Steel (Batch B) displayed an enhancement of fatigue life with LCF pre-training. Crack initiation and propagation was retarded in 316L (Batch C) by similar LCF pre-training. This behaviour was not observed in mild steel (C1020 and AS1214) or aluminium alloy (6060-T5). A martensitic strain induced transformation was found to be not responsible for the observed behaviour of 316L (Batch B). It is suggested that this behaviour supports the findings of fatigue crack growth experiments of 316L stainless steel (Batch A), i.e. that strain hardening is primarily responsible for fatigue crack growth retardation following tensile overload.

Acknowledgments

The project's supervisors, Professor Yuri Estrin and A/Professor Xiao-Zhi Hu, are thanked for their supervision. I would also like to thank Professor Yves Brèchet of the Institut National Polytechnique de Grenoble for his contributions over my PhD tenure.

In the department, I would like to thank the workshop personnel for their specimen manufacture. I would like to thank David Lee, Dr. Simon Drew and Dr. John Robinson for their timely technical advice on many issues. I would like to thank Dr. Martin Heilmaier (IFW-Dresden) for his contributions. I would also like to acknowledge my co-authors that contributed data for two of my seven publications. They are Roland Niefanger of Technische Universitat, Hamburg and David Bowman of UWA.

My thanks go to the Centre for Microscopy and Microanalysis at UWA for their assistance in production of the micrographs and their advice in production of the specimens for magnetic moment measurements. I would like to thank the Hi-Perm Laboratory (Physics Department, UWA) for their advice in magnetic moment measurements and specimen preparation. Finally, thanks are due to the University Library that has provided the multitudes of books and articles that I have requested over my PhD tenure.

Financial support through an Australian Post-Graduate Award (Industry) and the William Lambden Owen Scholarship is gratefully acknowledged. The APA (Industry) scholarship was made possible through the contribution of Rio Tinto, while the William Lambden Owen Scholarship was received from the University of Western Australia.

Finally, I would like to thank Sudabeh Wheatley, Shaday Wheatley, Maureen Stickney and Patrick Wheatley for all the support and encouragement they have given me.

For

Sudabeh & Shaday.

Contents

PhD Publications:

Note that all results presented in this thesis have already appeared in the following list of peer-reviewed articles.

1. Wheatley, G., Hu, X.Z. and Estrin, Y. (1997) Field emission scanning electron micrographs of fatigue crack growth in 316L steel following a single tensile overload. In: *Proceedings of the 1997 Workshop and State Conference of the Australian X-ray Analytical Association (WA) and The Western Australian Society of Electron Microscopy*, Perth, pp. 13-18.

2. Wheatley, G., Niefanger, R., Estrin Y. and Hu, X.Z. (1998) Fatigue crack growth in 316L stainless steel. *Key Engng Mater*. **145-149**, 631-636.

3. Wheatley, G., Estrin, Y., Hu, X.Z. and Brèchet, Y. (1998) Interaction between low cycle fatigue and high cycle fatigue in 316L stainless steel. In: *Proceedings of the Fourth International Conference on Low Cycle Fatigue and Elasto-Plastic Behaviour of Materials*. (Edited by Rie, K.-T., Portella, P.D.) Garmisch-Partenkirchen, Germany, pp. 567-572, Elsevier, Netherlands.

4. Wheatley, G., Estrin, Y., Hu, X.Z. and Brèchet, Y. (1998) Effect of low cycle fatigue on subsequent high cycle fatigue life of 316E stainless steel. *Mater. Sci. Engng A* **254**, 315-316.

5. Wheatley, G., Bowman, D., Estrin, Y., Hu, X.Z. and Brèchet, Y. (1999) Interaction between low cycle fatigue and high cycle fatigue in common metallic materials. In: *Proceedings of Fatigue 99*, (Edited by Wu, X.,-R, Wang, Z.,-G.) Beijing, pp. 1045-1050, Higher Education Press.

6. Wheatley, G., Hu, X.Z. and Estrin, Y. (1999) Effects of single tensile overloads on fatigue crack growth in a 316L steel. *Fatigue Fract. Engng Mater. Struct*. **22** 1041-1051.

7. Wheatley, G., Estrin, Y., Hu, X.Z. and Brèchet, Y. (submitted) Low and high cycle interaction in a 316L stainless steel, *Int. J. Fatigue*.

Oral/Poster Presentations

All results presented in this thesis have also appeared in the following list of Oral and/or Poster Presentations.

1. Departmental Seminar, Department of Mechanical and Materials Engineering, University of Western Australia, Perth, September 1997. (Oral)

2. State Conference of the Australian X-ray Analytical Association (WA) and The Western Australian Society of Electron Microscopy, Perth, 1997. (Oral)

3. Third International Conference on Fracture and Strength of Solids, Hong Kong University of Science & Technology, Hong Kong, 8-10 December 1997. (Oral)

4. Materials Institute of Western Australia, Annual Meeting of Researchers, Perth, Western Australia, July 1998. (Poster)

5. Monthly technical meeting of the Materials Society (IMEA) of the Institution of Engineers Australia (IEAust), Curtin University, Perth, Western Australia, 1998. (Oral)

6. Fourth International Conference of Low Cycle Fatigue and Elasto-plastic Behaviour of Materials, Garmisch-Partenkirchen, Germany, 7-11 September 1998. (Oral and Poster)

7. The 35th Annual Technical Meeting of the Society of Engineering Science, Washington State University, Pullman, Washington, Sept. 27-30, 1998 (Poster)

Nomenclature

Latin alphabet

a	crack length, notch length
B	specimen thickness
B*	critical thickness above which plain strain conditions prevail
C	fractional life sum
C(a)	elastic compliance (as a function of crack length)
C'(a)	first derivative of elastic compliance with respect to crack length
$C_{co}(a)$	experimentally measured compliance for open crack
C_{DCC}	middle part of compliance curve (Discontinuous Crack Closure)
COD	crack opening displacement
C_{PICC}	lower part of compliance curve (Plasticity-Induced Crack Closure)
CT	compact tension
da	increment of crack length
da/dN	fatigue crack growth rate
dN	cycle number increment
E	Young's Modulus; also energy associated with magnetic moment
H	magnetic field intensity
J	J integral
K	stress intensity factor; fracture toughness; constant
K_c	Plain stress fracture toughness - specimen width dependent
K_{IC}	Plain strain fracture toughness - specimen width independent
M	magnetic moment
n	number of fatigue cycles
N	number of fatigue cycles
N_F	number of fatigue cycles to failure

P	load (kN)
P_c	critical load (used to calculate K_c)
R	load ratio = minimum load divided by maximum load during fatigue
r_c	radius of residual compressive zone
r_p	radius of plastic zone
t	time
T	temperature
W	length of specimen from loading line to back face
x, y, z	coordinate axis notation
Y	geometry factor

Greek alphabet

Δa	crack tip displacement after overload
ΔK	stress intensity factor range
$\Delta\sigma_P$	Plastic strain range
$\Phi(a)$	compliance function defined by C(a) and $C_{CO}(a)$ (see text)
α	a/W ratio
δ	vertical displacement at notch mouth
ε	Strain
Φ	Phi function
ν	Poisson's ratio
θ	Angle measured from plane of crack
σ	Stress
σ_Y	Yield strength
ρ	radius of curvature

Superscripts and subscripts

av	average
e	elastic
f	failure
i	mode I
i, j	indices of tensor, with reference to respective coordinate axes
max	maximum
min	minimum
m, n	exponent in a power law
P	plastic
th	theoretical
y	yield

Chapter One: Introduction

Fatigue is a progressive damage process in a structure subjected to cyclic loading. This load may or may not exceed the yield strength of the material. The plastic deformation that results from an excursion beyond the yield strength may be confined to a small part of the structure (i.e. at a crack tip) or the entire structure may be grossly deformed.

Knowledge of fatigue involves a combined effort of two disciplines: mechanical and materials engineering. The occurrence of fatigue in industry is a problem that is often dealt with by the mechanical engineer. The study of fatigue for the mechanical engineer centres on crack propagation rates and fatigue life. Since microstructure is a determining factor in fatigue, materials engineering aspects need to be investigated. The instruments for a materials oriented study of fatigue include the field emission scanning electron microscope (FESEM), magnetic moment measurements and further specialised techniques, alongside mechanical testing.

The first published paper on the effects of metal fatigue was by Albert in 1838. It was based on a study that is believed to have been conducted in 1829 [1]. The notion of failure of metals as a result of 'fatigue' loading was first coined by Poncelet [2] in 1839. As previously mentioned, industrial fatigue failure is often catastrophic in nature. The failures are often dramatic and, unfortunately, can lead to loss of human life. A railway accident in Versailles, France in 1842 was of this type and sparked the first detailed scientific study of fatigue. In 1843, W.J.M. Rankine noted the danger of stress concentrations [3]. It is now recognised that avoiding stress concentrations is the most important aspect of good fatigue design. Wohler first noticed the loss of strength as a result of fatigue loading in 1860 [4]. This is now known as strain-induced softening but some materials do exhibit strain-induced hardening. In his study of 1864, Fairbairn [5] concluded that a maximum cyclic load of only one third of the ultimate strength would still cause the eventual failure of the component. Study of life calculations was initiated

by Gerber [6] and Goodman [7], Bauschinger extended the work of Wohler by identifying both cyclic softening and hardening [8]. Major works were published in 1900 by Ewing and Rosenhain [9] and in 1903 by Ewing and Humfrey [10]. Observations of slip bands progressing to cracks were made. Surface damage (now referred to as extrusions and intrusions) was also noted. Basquin [11] showed in 1910 that the presentation of a double logarithmic S-N plot displayed a linear relationship between the stress amplitude (S) and the number of cycles to failure (N) over a significant strain range. Palmgren [12] and Miner [13] published fatigue damage accumulation models in 1924 and 1945, respectively. Langer presented a variable amplitude fatigue study in 1937 [14]. Neuber published results from notch effect studies in 1946 [15]. Zappfe and Worden first documented fatigue striations in 1951 [16]. Coffin [17] and Manson [18] both noted the connection between plastic deformation and cyclic damage in 1954.

Miner's rule states that the damage fraction at a given stress amplitude is linearly proportional to the fractional life: the number of cycles actually spent at that stress amplitude divided by the would-be life at that stress amplitude. The latter quantity can be taken from the appropriate S-N curve. Miner's rule takes the following form:

$$\sum_i \frac{n_i}{N_i} = C \tag{1.1}$$

where: n_i = number of cycles of stress in the i-th condition determined by the stess amplitude,

N_i = life (number of cycles to failure) at that stress amplitude and

C = total accumulated damage sum

It is assumed that failure occurs when C = 1. However, the constant C is experimentally found to range substantially from unity [19]. The life to failure can be estimated by adding up the fractional lives, subtracting the result that from the damage sum, C. ASTM guidelines [20] recommend that this damage sum be equated to 1. In other words, the life of a material is tested in the laboratory and a structure is estimated to have a certain life based on that data. However, the sum of fractional lives is generally not equal to 1 and as stated above, the constant C can depart from that value quite appreciably. The total life depends on what loadings the material is exposed to, particularly on the sequencing of loadings. It is assumed that the damage created during a certain loading is not dependent on when that loading pattern took place in the life history of the structure.

Non-linear damage hypotheses exist but due to their complexity, a linear rule is still attractive for use by engineers.

Irwin developed the linear elastic fracture mechanics approach and introduced the stress intensity factor, K, in 1957 [21]. In 1960, Forsyth and Ryder correlated the fatigue crack growth rate with fatigue striations [22]. In 1961, Paris parameterised crack growth rates with K [23]. An interesting and often humorous account of Paris' early work can be found in the literature [24]. The next step was taken by Elber in 1970 [25] when he established that the fatigue crack growth rate was dependent upon the effective K, rather than K proper. This was due to the plastic deformation at the crack tip causing the fracture surfaces to contact each other prior to the complete removal of tensile load. In the early 1980's, Ritchie extended the notion of crack closure to include many other possible reasons for this effect [26, 27, 28]. Elber's result was then termed plasticity-induced crack closure. One major consequence of this work was that the prior loading history was observed to affect the fatigue crack growth rate. As a result, earlier studies that examined fatigue crack growth under constant amplitude conditions were superseded by studies where variable amplitude fatigue loading exists. The role of residual compressive stress has been a subject of some controversy and disagreement between some researchers as to its effect. Shin [29] argued against the effect of residual compressive stress as immediate crack retardation was not observed. However, the presence of a damage zone ahead of the crack tip observed by Damri [30] and others can explain the transient acceleration without discounting the presence of the residual compressive zone observed by Suresh [31], among others. Observation of the material at the crack tip by Hu and Mai [32] have shown the large contribution made by the material in this area that is added to crack closure factors. The fatigue life can be extended by fabricating a material that encourages crack deflection, cf. Suresh [31]. Miller [33] observed that mixed mode crack growth needs to be understood because crack growth in the presence of material defects may be different from Mode I. Miller further notes [34] that prior loading history is often ignored in experimental studies.

Chapter Two: Literature Review

2.1 Fatigue Crack Growth

Crack growth occurs through localised plastic deformation within slip bands near the crack tip. Uniaxial fatigue crack growth is divided into distinct stages. The first stage is characterised by crack growth occurring in the direction of the primary slip system by single shear in a given grain. Due to grain misorientation in a polycrystal, this leads to a zig-zag path of a crack. The crack and the plastic deformation zone ahead of the crack tip are a few grain diameters long. After the crack grows to a larger length or at higher stress concentrations, the size of the plastic zone at the crack tip is many grain diameters.

Stage II crack growth [35] is associated with deformation along two slip systems. The result is a crack path normal to the applied stress direction. The yielding is considered small scale when the plastic zone is much smaller than the crack length. It has been observed that the fatigue crack growth rate in region II is relatively insensitive to microstructure and monotonic deformation properties. This is in contrast to the fatigue crack growth rate in region I. The fatigue crack growth rate in region II is relatively constant for similar materials. In fatigue loading, cyclic flow properties control fracture. Striations are visible marks on the crack surface that are parallel to the crack front. They are an often-observed phenomenon associated with Stage II crack growth. Striations were first observed in 1951 [36] and are found in many ductile alloys and pure metals. A striation may form every cycle and a count of the striations gives an estimate of the fatigue life of the failed component. Steels generally do not exhibit this behaviour. If crack growth is allowed to continue sufficiently long then failure of the component will occur.

Surprisingly, there is still some controversy about the exact mechanism of fatigue crack

growth. The plastic blunting model of Laird [37, 38].is quoted in the literature a great deal. The model suggests that as the load increases, the crack tip is blunted. Due to the stretch zone as a result of the blunting, the crack grows slightly. Local slip follows the plane of maximum shear stress and therefore occurs at an angle of ±45° to the plane of crack propagation. The direction of slip then reverses during the unloading fatigue cycle, the crack tip folding inward. This process occurs in every fatigue cycle. One upshot of this model is that a striation should be formed in every fatigue cycle, but this has been observed not to occur [39]. The model has been seen to be deficient because Laird's blunting mechanism should be related to the change in crack tip opening displacement. That implies that the fatigue crack growth rate should be directly proportional to $(\Delta K)^2$. Experimentally derived Paris exponents, however, vary between 3-4 for metals. A possible interpretation of this discrepancy is that the model is incorrect, but there may be other reasons for it.

Another model is the damage accumulation model. In this model, it is viewed that the fatigue process induces damage in the material directly ahead of the crack tip. When a certain level of damage is attained, the fatigue crack grows incrementally. A model by Vasudeven, Sadananda and Louat [40] based upon dislocation motion in the plastic zone has been put forward. An interesting consequence of the model is that the contribution of crack closure is considered, at the very least, to be much less than previously thought. Its major proponent, Ritchie, has vigorously defended the influence of crack closure [41].

For high ΔK levels that occur during region III, the fatigue crack growth rate accelerates. It is believed to occur partly due to both fracture and fatigue mechanisms operating concurrently. A number of different mechanisms, including shear, microvoid coalescence and striations may be operative. Microvoid coalescence and/or shear dominate the final stage that culminates in fracture.

The process of fatigue damage and ultimate failure has a probabilistic nature that begins from the atomic level and continues up to the final specimen or machine form. For this reason, considerable statistical scatter exists. For the same testing conditions, the cyclic durability can change by an order of magnitude or more [46].

2.2 The Palmgren-Miner Approach

With the S-N curve, the fatigue life is measured from initiation of fatigue loading until the specimen fractures. The crack growth phase is not differentiated from the other phases of fatigue life that includes the number of cycles to induce microscopic damage and that of growth of the major crack to ultimate failure. The fractional life that is expended to produce a dominant crack can vary from 0-80% of the total life. The main division in fatigue testing within the S-N curve approach is into low and high cycle fatigue. Low cycle fatigue (LCF) occurs within stress or strain ranges where large-scale plastic deformation prevails. High cycle fatigue (HCF) occurs where elastic deformation predominates. Failures that occur before approximately 10^3 cycles are deemed low cycle fatigue cases, whereas those above this level are referred to as high cycle fatigue.

S-N plots are constructed to show the life to failure at each particular stress or strain amplitude. However, structures are rarely exposed to constant amplitude fatigue loading in reality. In order to approximate the level of fatigue damage a material has sustained, Palmgren [12] and Miner [13] independently developed the cumulative damage rule. The number of cycles a material sustains under a certain loading is divided by the predicted life of the material at that loading taken in isolation. The fractional lives, calculated for all loading conditions involved, are summed. The damage accumulation (associated with fatigue loading) is assumed to be linear. It is assumed that the order of different loading conditions does not affect the remaining life. Studies indicate that only with a confidence level of 0.05, can it be said that the loading history does not influence the total fatigue life [46]. The final assumption is that failure occurs when the sum of fractional lives reaches unity. These assumptions do not hold in many instances. Despite this, the Palmgren-Miner rule-is-the cornerstone of residual life assessment in ASTM standards.

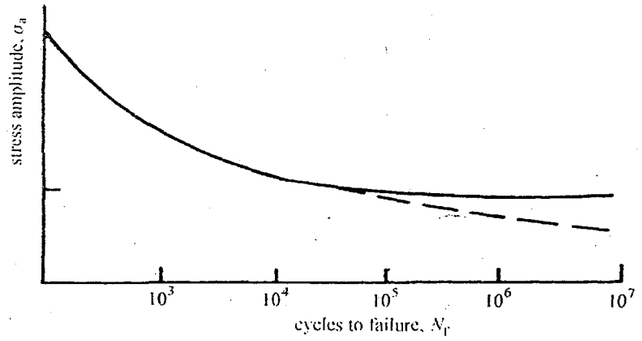

Figure 2.1 - S-N curve (schematic) [19].

The Palmgren-Miner rule can be derived by integration of the appropriate fatigue crack growth rate expression for high cycle fatigue at different stress ranges or during low cycle fatigue. This calculation shows that, at failure, the fatigue life summation is equal to unity [42]. The mathematical proof is attached as an Appendix. However, by the mere fact of integrating the appropriate fatigue crack growth rate expression, the Palmgren-Miner rule is therefore implicitly concerned with fatigue crack propagation. The major part of the fatigue life that is taken up by crack initiation is neglected. Based on this, the success of Miner's rule is somewhat surprising [42]. However, the delineation between crack initiation and growth has been well researched [43].

Deviations from Miner's rule may occur when one considers a fatigue life being taken up by two different stress range applications. Generally, it is observed that if the higher stress range is applied first, followed by the lower stress range, then the fatigue life summation is less than one. If the lower stress range is applied first, then the fatigue life summation is greater than one. However, the argument for this behaviour relies on the first stress range initiating a crack. The second stress range then does not have to initiate a crack and Miner's rule is altered from unity. The first stress range, prior to initiating a crack, simply cold works the specimen. Chaboche [44, 45] reports that for 316L, a number of high level load cycles increase the fatigue life at a subsequent lower level of load.

Experimental results show a large scatter, not a perfect fatigue life summation equal to one [46]. This scatter is due to the statistical scatter of the fatigue resistance of the samples. This scatter is compounded by the scatter within the loading applied to the specimens. Large numbers of specimens must be tested to fully account for the statistical variations. The conclusion that damage increases linearly with exposure to

fatigue is also highly debatable. Non-linear cumulative models of damage are able to support strengthening effects by preliminary fatigue loading [46].

2.3 Fracture Mechanics

2.3.1 Linear Elastic Fracture Mechanics

Fracture mechanics that includes the assumption that the material is obeying Hooke's law is grouped within linear elastic fracture mechanics (LEFM). Essentially, plasticity is ignored in this division of fracture mechanics. The assumptions of linear elastic fracture mechanics are:

1. Defects and cracks are present in materials and structures.
2. The fracture toughness is a material constant.
3. The crack tip is defined as being infinitely sharp and the crack surfaces are free of any stresses (e.g. residual stresses).

The stress distribution at the crack tip is characterised by the stress intensity factor, K. The stress intensity factor range is dependent on the maximum and minimum loads experienced during the constant fatigue applied amplitude and by the crack length.

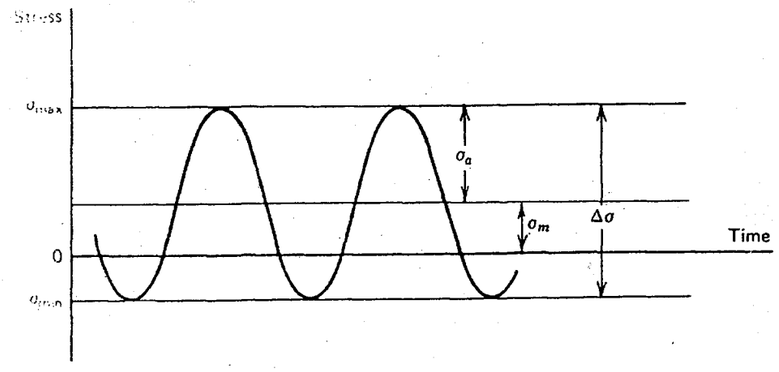

Figure 2.2 - Stress range [49].

This curve is dependent on similitude being maintained throughout crack growth. Consequently, the crack tip conditions can be uniquely defined by a single factor, such as the stress intensity factor. This would imply that K_{MAX} and K_{MIN} are kept constant. This means that the stress intensity factor range at which fatigue crack growth occurs at is kept constant. Tests carried out with similitude being maintained are fairly well understood.

However, there are some difficulties with this concept. The above description presumes that the material is uniform throughout. If a compliance measurement is taken, one can see using energy methods how the stress intensity is also dependent on Young's modulus [47]. Hence, any change in the material and the stress intensity would also change.

If the plastic deformation at the crack tip exceeds a certain level, K cannot be used to characterise the crack tip stress distribution. Other parameters can be employed for these conditions. If the fatigue crack growth rate is plotted against the stress intensity factor range, ΔK, the following plot may be generated.

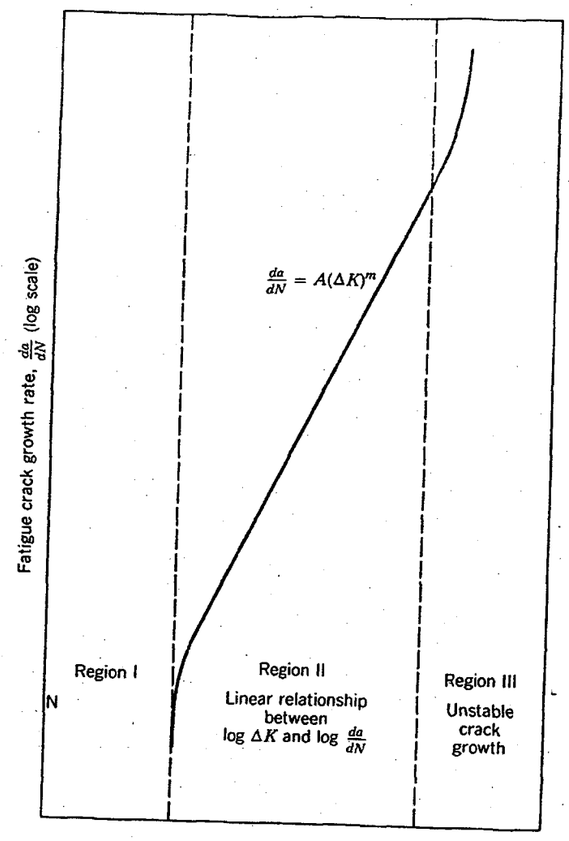

Figure 2.3 - Paris curve with mechanisms of crack growth for each stage. The major contributors toward these mechanisms are also presented.

The linear behaviour at medium ΔK levels is clearly observable in the double logarithm plot. Paris [23] suggested the following relation to describe the stable crack growth associated with region II fatigue crack growth:

$$\frac{da}{dN} = C\Delta K^m \qquad (2.1)$$

The constants C and m in the Paris law are material parameters. It should be noted that history effects are ignored in this formula. The Paris law only applies to constant amplitude fatigue crack growth.

Shortly after the breakthrough by Paris, Elber [48] was able to shed more light on the effects of altering the ratio between the minimum and maximum fatigue load (ie. the R ratio). Elber also explained the occurrence of a non-linear section of the sigmoidal fatigue crack growth curve (Fig. 2.12). Through the use of compliance plots, Elber showed that the experimentally determined compliance approached theoretical values at high loads, but at low loads the compliance approached that of an uncracked specimen.

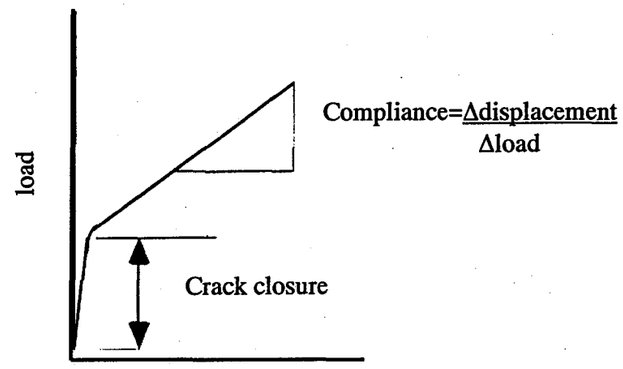

Figure 2.4 - Compliance plot of a specimen containing a crack.

Elber attributed this behaviour to the crack fracture surfaces contacting each other while some tensile force continued to be applied. Since the specimen was no longer experiencing the tensile load below the level at which the fracture surfaces were expected to be in contact, it was reasoned that the stress intensity range applied to the specimen was not in fact fully transmitted to the crack tip. This implies that the driving force for crack growth was less than the nominal one. Elber defined an 'effective' stress intensity range.

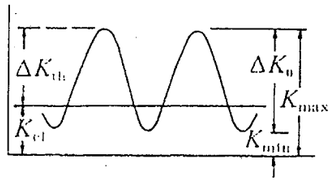

Figure 2.5 - Stress intensity factor range theoretically applied (K_{max}-K_{min}) versus the effective stress intensity factor range (K_{max}-K_{cl}) [49].

Extensive research confirmed the occurrence of crack closure. Suresh and Ritchie [50] discussed five mechanisms that would result in the occurrence of crack closure, cf. Fig. 2.14.

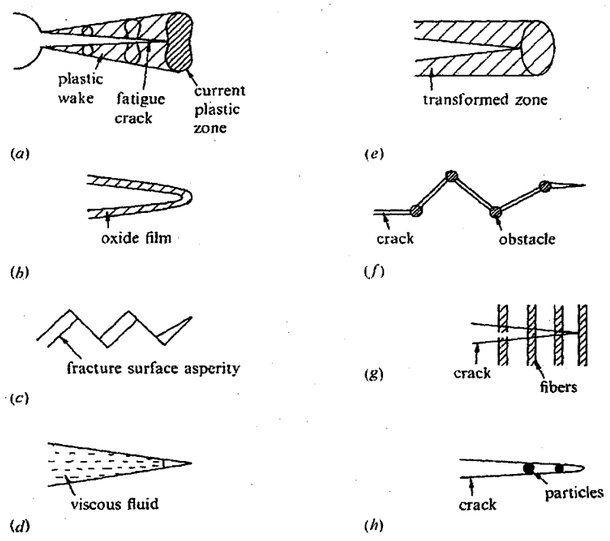

Figure 2.6 - Types of crack closure [19]. Plasticity-induced closure (Case (a)) is of particular relevance to this thesis.

Plasticity-induced crack closure (Case (a)) is what Elber originally noticed during his initial research. It is caused by residual stresses resulting from plastic deformation in the plastic zone and leading to partial contact of the sides of the crack.

Viscous fluid-induced crack closure can be used in the repair of fatigue cracks by the introduction of foreign materials within the crack [51].

Schijve [52] appears to be the first to observe crack retardation following the application of a single tensile overload, cf. Fig. 2.15.

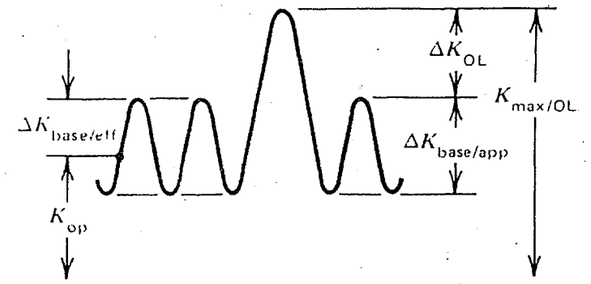

Figure 2.7 - A single tensile overload [49].

Von Euw [53] noticed that the fatigue crack retardation did not set in immediately after the overload, but rather occurred after the crack had grown approximately through the overload plastic zone. Ellyin noted [54] that Elber [25] used crack closure to explain the retardation of fatigue crack growth following an overload. However, Elber suggested that the crack opening stress was greater for the stabilised crack (prior to overload) than after overload. Ellyin therefore concluded that an acceleration of crack growth must occur prior to an overall retardation.

The transient acceleration was explained by Carlson [55] in the following manner. The tensile overload blunts the crack and therefore increases the effective stress intensity factor range. A report by Kumar [56] showed that following a tensile overload, the crack closure level did in fact increase. However, results from Tsukuda [57] displayed transient acceleration with the load ratio, R, approximately equal to 0. The inconsistent findings in regard to closure may be the result of the difficulty in measuring [58].

The theoretical relation Φ is dependent on crack length and offers some insight into the reason for the acceleration. The equation is based on Linear Elastic fracture mechanics. The theoretical compliance may be greater, the same or less than the experimentally determined compliance value.

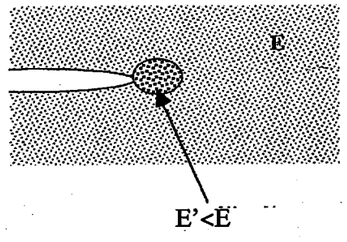

Figure 2.8 - Fatigue damage zone at crack tip.

The former case can be interpreted in terms of the experimentally measured Young's modulus being less than the theoretical one, ie. the material is effectively less stiff, which is believed to be caused by a damaged zone at the crack tip that has a Young's modulus smaller than the surrounding material. If the experimental compliance is greater (ie. the effective Young's modulus is smaller) than that expected from theory, the damaged zone effectively 'lengthens' the crack. It should be noted that the damage zone (Fig. 2.27) is not identical with the plastic zone mentioned above. The distinction between the two will be discussed below. In the course of monotonic loading, Young's modulus is usually not changing. However, strain hardening does occur and the endurance limit for subsequent cyclic loading increases.

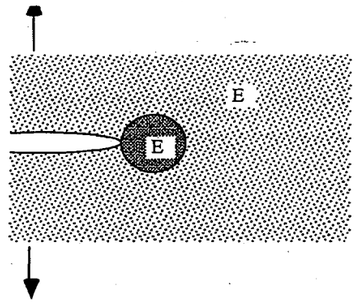

Figure 2.9 - Plastic deformation at crack tip as a result of tensile overload. Young's modulus within the plastic zone is considered not to differ from that outside the plastic zone.

During fatigue, a fatigue damage zone (FDZ) is established ahead of the crack tip. The FDZ is an area where damage is initiated. It is believed that the FDZ is enclosed within the plastic zone, as schematically depicted in Fig. 2.30.

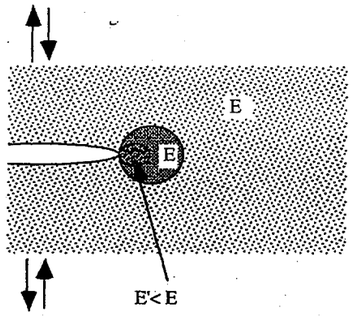

Figure 2.10 - Fatigue damage zone within the plastically deformed zone at the crack tip. Young's modulus within the fatigue damage zone, E', is considered to be smaller than E.

Skorupa [59] noted that depending upon the combination of loading, material, specimen, microstructure and environment, identical loading sequences can produce

either retardation or acceleration in the fatigue crack growth following a tensile overload. In another contribution, Skorupa [60] concluded that plastic straining at the crack tip can account for the majority of experimental results. Plastic straining at the crack tip results in a number of effects. These include crack tip blunting, plasticity-induced crack closure (PICC), as well as strain hardening an residual stresses in the material ahead of the crack tip. Modelling of the experimental results is continuing [61].

Crack tip blunting has two opposing effects upon the fatigue crack growth rate. Christensen [62] noted that a blunted crack tip was similar to a notch and therefore a certain number of cycles would be required to re-initiate a fatigue crack. However, Fleck [63] observed that a stress relieving a specimen following a single tensile overload did not result in fatigue crack retardation. This indicates that the blunted crack tip did not cause the retardation as the stress relieved specimen still had a blunted crack tip. This seems to indicate that the removal of some crack closure by blunting (resulting in acceleration of the fatigue crack growth) dominates over the contribution of crack blunting that requires re-initiation of crack propagation.

A tensile overload results in increased plastic deformation at the crack tip. After removal of the overload, the surrounding elastic material produces a compressive stress in the material in the plastic zone [64]. Davidson [65] observed that the level of residual stress approximates the material's yield stress and the size of the residual stress affected zone is larger after an overload than before it. Schijve [66] argued that the compressive stresses reduce the effective stress intensity factor range and hence cause crack growth retardation.

PICC comes into effect after the initial acceleration period. The residual compressive forces, while decreasing the stress intensity factor range, also cause the crack faces to contact more than in the absence of an overload. Fleck [63] observed the occurrence of discontinuous crack closure (DCC), leading to a faster crack growth than predicted by common crack closure models. Fleck suggested that this results from the crack flanks being open but the crack surfaces still touching at the crack tip.

Jones [67] reasoned that the plastic deformation of the material ahead of the crack tip could cause strain hardening there. This would then lead to fatigue crack growth retardation. Experimental evidence was presented to substantiate this mechanism [68]. It was suggested that this small zone of hardened material, surrounded by softer material, impedes crack growth [60]. In that paper, Skorupa also observes that the material ahead of the crack tip can be thought of as experiencing low cycle fatigue.

2.3.2 Elastic-Plastic Fracture Mechanics

If the size of the plastic zone ahead of the crack tip is of a size that precludes the use of LEFM, then Elastic-Plastic Fracture Mechanics (EPFM) may be used. The parameter used for the characterisation of fracture in real ductile materials is the J integral developed by Rice [69]. Another method of characterisation is through measurement of the crack tip opening displacement (CTOD). The CTOD provides information on the size of the region at the crack tip where strain deformation is dominant. Through this measure, a critical CTOD when fracture occurs can be observed. This measure provides a pleasing link between microscopic failure processes and the measure of the fracture toughness. The Tomkins model [70], which models striation formation on the intense plastic flow at the tip of the fatigue crack, is another basis for EPFM.

2.3.3 Mixed Mode Fracture Mechanics

LEFM and EPFM cannot cope with combined mode loading situations. The application of different modes of loading may have a dramatic effect in the crack growth. Solutions for mixed mode loading in the mode I and II situation and for deflected and branched cracks have been developed.

Chapter Three: Experiment

3.1 Summary

3.1.1 Types of experiments

i. Fracture toughness tests,

ii. Fatigue crack growth tests (including application of overload),

iii. Compliance measurements,

iv. Observation of crack tip and wake through FESEM,

v. High strain/low stress tests, and

vi. Magnetic moment measurements.

3.1.2 Techniques

i. Fracture toughness tests were carried out as per ASTM standard E399-90.

ii. Fatigue crack growth tests were carried out as per ASTM standard E647-93.

iii. Compliance measurements were conducted as per ASTM standard E647-93. Essentially, a COD (crack opening displacement) gauge was used to determine COD as a function of applied load. From these plots, the load at which crack opening occurred, as well as the compliance of the material, could be determined.

iv. Observation of crack tip and wake through FESEM was conducted with the assistance of staff at the UWA Centre for Microscopy and Microanalysis (Mr. John Hillyer).

v. High strain/low stress tests were conducted by subjecting standard specimens (ASTM standard E606-92) to a high strain regime followed by a low stress

regime. The purpose of this series of experiments was to expand upon results obtained on CT specimens. For this reason, following the high strain regime applied to the specimens, notches were introduced into the standard specimens. I would like to thank Professor Yves Bre chet for the suggestion of this modification to the standard specimen shape. The low stress regime was then applied and continued until failure.

vi. Magnetic moment measurements were conducted under the direction of staff/students of the UWA Hi-Perm Laboratory (Mr. Leonard Wee, Mr. Rob Woodward and Professor Robert Street). Essentially, small cylinders were removed from the central region of the standard test specimens. These small cylinders were then tested for the presence of magnetic material. The presence (or change in concentration) of magnetic material would indicate the occurrence of a strain induced phase transformation.

3.1.3 Specimen shapes

i. Standard CT specimens were used as per ASTM standard E399-90.

ii. Standard CT specimens were used as per ASTM standard E647-93.

iii. Compliance measurements were conducted upon Standard CT specimens were used as per ASTM standard E647-93.

iv. FESEM observation of the crack tip and crack wake required the sectioning of areas of interest from the CT specimens. This is required due to FESEM dimensions. The specimens were rectangular in shape and measured approximately 5X5X10mm.

v. Standard 'hourglass' specimens, as per ASTM standard E606-92, were used. Following the application of a high strain regime, a notch was introduced into the middle of the specimen. This was done to approximate the notch of a CT specimen.

vi. Specimens for magnetic moment determination were of a cylindrical shape and measured approximately 2mm in diameter and 5mm in length. They were removed from the centreline of the 'hourglass' specimens. A specimen was removed from the threaded and the gauge length sections of the 'hourglass' specimens.

3.1.4 Materials

i. Fracture toughness tests were determined for 316L stainless steel (Batch A - CT specimens).

ii. Fatigue crack growth tests were conducted upon 316L stainless steel (Batch A - CT specimens).

iii. Compliance tests were conducted upon 316L stainless steel (Batch A - CT specimens).

iv. FESEM observations were conducted upon 316L stainless steel (Batch A - CT specimens).

v. High strain/low stress tests were conducted on 316L stainless steel (Batch B and C). In addition, aluminium alloy 6060-T5 and two mild steels (C1020 and AS1214) were tested. The AS1214 material was tested in the as-received and the normalised conditions.

vi. Magnetic moment measurements were conducted on 316L stainless steel (Batch B).

3.2 Fatigue Crack Growth Investigations

The 316L austenitic stainless steel (Batch A) was available in the rolled bar form. The 'L' in the label refers to the low carbon variety of this type of steel. Testing was done in the as-received condition with the mechanical and chemical properties summarised in Table 3.1.

Table 3.1

Chemical and mechanical properties (316L stainless steel – Batch A).

C	Si	Mn	P	S	Ni	Cr	Mo	N
0.025	0.41	1.3	0.031	0.003	10.62	16.72	2.01	0.032

Yield stress [MPa]	U.T.S. [MPa]	Elongation [%]	Hardness [HR]
334	588	62.9	87

Compact Tension (CT) specimens of standard geometry (Fig. 3.1) were manufactured from a bar.

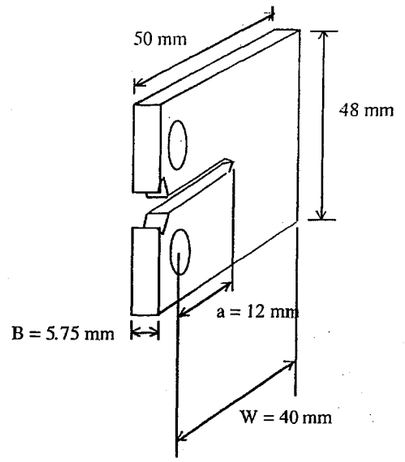

(a)

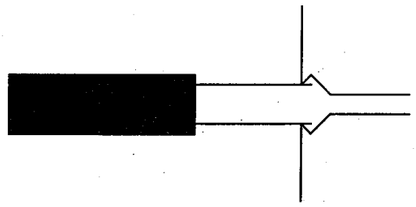

(b)

Figure 3.1 – (a) CT specimen dimensions (b) Crack opening displacement (COD) gauge.

The specimen width (W) was 40 mm. The thickness of the specimens was 6 mm. An a/W ratio of 0.3 was used for the experiments. Notches were manufactured parallel to the bar's longitudinal axis (ie. T-L orientation), cf. Fig. 3.2. Holes of 5mm were installed such that bars could be inserted for load application.

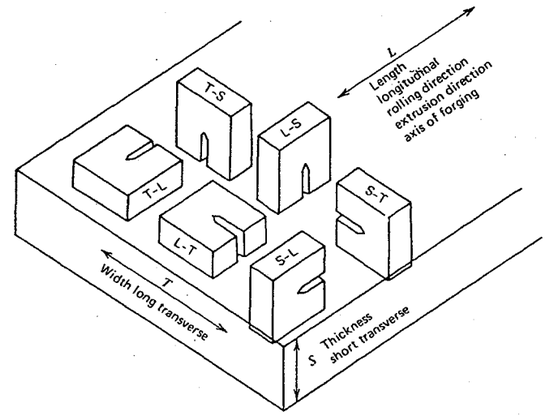

Fig. 3.2 - Nomenclature coding for specimen orientation relative to stock [49].

In order to facilitate observation and optical measurements of crack length, one side of the specimen was polished. This was done in a gradual, step-wise fashion down to 1 μm diamond paste as a polishing medium.

Optical measurement of crack length was carried out in all cases via a travelling optical microscope attached to the servo-hydraulic Instron 8501 testing machine that was used for all tests (Fig. 3.2).

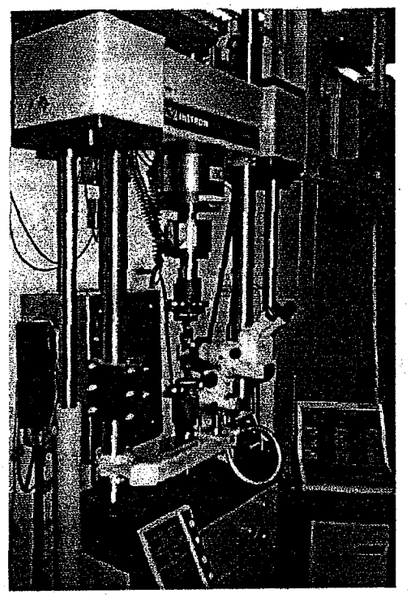

Figure 3.3 - Instron 8501.

The optical crack measurement technique was used to avoid any interference of overload with crack length measurement using elastic compliance. The accuracy of

crack length measurement was ±0.02mm. Crack front shape was considered to be unchanging throughout crack growth.

The testing procedure began with a fracture toughness test. This was done in order to determine the critical load, P_r (used to calculate K_c). The procedure followed was to install a fatigue crack in the specimen to a minimum length of 1.3 mm. This necessitated using a step-down method to allow crack initiation from the notch. Since the notch is more blunt than the fatigue crack tip, a much larger maximum load is required during the fatigue cycling to allow crack initiation. After initiation, the maximum load is reduced so that excessive plastic deformation is avoided. For 316L investigated, this final fatigue applied amplitude had a maximum load of 3.0 kN, a frequency of 20 Hz and a load ratio of R = 0.1. The load was then increased at a constant rate to obtain a load vs. strain diagram. The 0.2% offset rule was used to determine P_c. The fracture toughness was found to be 32.9 MPa$\sqrt{m}$ [71]. Using this value, the critical thickness, B*, was calculated according to the standard. The material at the surface of a specimen will always be subjected to plane stress due to the lack of triaxialty. However, a critical thickness exists beyond which plane strain condition prevails. The B* value obtained for the 316L material was found to be greater than the actual specimen thickness. This means that the plane stress rather than plane strain condition applied. That is to say, it was the fracture toughness K_c that was determined, rather than K_{1C}.

The next step was to grow similar length fatigue pre-cracks into CT specimens with a notch length of 12mm. This pre-crack was 1.3 mm long. After this fatigue loading, the specimens were subjected to different types of overload and then fatigue cracks were grown further under the same cyclic loading conditions as prior to the overload. The fatigue applied amplitude and the loading history were similar in all cases [121].

The specimens were divided into four groups. In the first group, no overload was applied. That is, the same fatigue applied amplitude was continued until failure. Optical measurements, made by means of a travelling microscope, were taken about every 5000 cycles. The remaining groups of specimens (i.e. two specimens per group) were subjected to varying levels and time periods of tensile overload. One set was overloaded to 90% of P_c (4 kN) (P_c used to calculate K_c) for either 1 minute or 1 hour. The next set was overloaded to 110% of PC (5 kN) for either 1 minute or 1 hour. The final set was overloaded to 120% of P_c (6 kN) for the same time periods. The same fatigue applied amplitude as prior to overload was then applied and the crack growth measured. The crack length measurements were smoothed using a four point travelling average

technique. In the first round of experiments (i.e. the first specimen from each group), apparent crack growth acceleration following re-establishment of the fatigue applied amplitude was noted. If the crack growth measurements were not averaged, this initial acceleration could be observed. In the later experiments (i.e. the second specimen from each group), the crack growth measurements were taken at much shorter intervals following reinstatement of the fatigue applied amplitude so that this acceleration was discernible in the averaged crack growth results, as well.

In these later experiments, compliance measurements were also taken concurrently with crack length measurements. The accuracy of compliance measurement was ±0.001mrn/kN. An Instron CMOD (crack mouth opening displacement) strain gauge (gauge length: 10mm, travel distance: 4mm) was attached to the front face of a specimen. This type of strain gauge is the most commonly used due to ease of its implementation, as only one gauge is required and also since it is insensitive to crack tip position. Further, the fact that it returns averaged through-thickness values complements nicely the surface crack length measurements. As outlined in Section 3.1, following the application of a tensile overload, the same fatigue applied amplitude as prior to overload was applied again. After the qualitative observation of fatigue crack growth acceleration, the experiments were repeated and the interval between crack length and compliance measurement was reduced drastically. In the first 300-400 μm of crack growth, compliance measurements were taken approximately every 100 μm. After this first crucial crack growth, measurements were taken approximately every 0.5 mm. The results of the experiments are grouped into low, medium and high overloads. These divisions are made on the basis of the presence or absence of certain sections of the compliance curve. The compliance plots show the presence or absence of Plasticity-Induced Crack Closure (PICC), Discontinuous Crack Closure (DCC) and Crack Opening (CO), cf. Section 2.4 where this terminology was introduced. Compliance plots were produced using a Lloyd PL3 chart recorder. No mathematical data processing was required as the plots clearly show piecewise linear behaviour with single, dual or triple slope characteristics. The compliance was measured directly from the chart. The elastic region was the straight section of the curve nearest to the origin. The Discontinuous Crack Closure region (if present) was the second straight section of the plot while the Crack Opening portion was the last straight section of the curve, cf. Fig. 4.9. This interpretation of the three stages of the compliance curves will be discussed in Chapter Five.

To assist in determining the reason behind the transient acceleration, two further groups of specimens were produced for the purpose of field emission scanning electron microscope (FESEM) observation. The first group consisted of 3 specimens with fatigue pre-cracks of 6 mm in length. These were subjected to overloads of 130% of P_c for 1 minute. The second group consisted of specimens that had fatigue pre-cracks of 1.3 mm. A sinusoidal applied amplitude between 0.4-4 kN at 20 Hz was applied. These specimens were subjected to tensile overloads amounting to 45%, 75%, 80% and 200% of P_c. The overloads of 75% and 80% of P_c were over the fatigue applied amplitude maximum. These two groups of specimens were analysed under the FESEM. The specimens were sectioned to allow installation in the FESEM. The sectioned specimens were ultrasonically cleaned in acetone and carbon coated to reduce edge highlighting and also to reduce the formation of scanning squares on the specimen surface. These squares are produced as a result of the electron beam burning oil vapour onto the surface. The oil vapour is a result of the final stages of vacuum production in the FESEM.

3.3 High Strain-Low Stress Interactions

This segment of the investigation was conducted in order to more closely examine material changes as a result of fatigue loading. The investigation into the effect of tensile overloads on fatigue crack growth rates showed that fatigue caused damage to the material. However, the scale of the damage was very small. The effects involved were studied on tensile specimens subjected to fatigue loading. In addition, there is a great need for studies into the interaction between different modes of cyclic loading. In this project, the effect of low cycle fatigue on subsequent fatigue life under high cycle fatigue conditions was investigated. Different materials were used for comparison purposes.

Initially, standard 316L 12.7mm round bar was used in the as-received condition (Batch B). Two batches of 316L were tested (Batch B and C) with the chemical and mechanical properties given in Tables 3.3 and 3.4.

Table 3.2

Chemical composition of 316L (Batch B and C).

316L	C	Mn	Si	P	S	Ni	Cr	Mo	Cu	N ppm
Batch B	0.022	1.38	0.390	0.037	0.012	11.50	17.49	2.15	0.110	270
Batch C	0.020	0.61	0.42	0.024	0.026	11.93	17.26	2.05	-	0.050

Table 3.3

Mechanical properties of 316L (Batch B and C).

316L	yield strength (MPa)	tensile Strength	elongation (%)	area reduction (%)	hardness (HB)
Batch B	509	687	37.4	68.2	207
Batch C	632	741	40	75	217

Later, other materials were also tested. These materials included aluminium alloy 6060-T5 and two mild steels (C1020 and AS1214). The AS1214 material was tested in the as-received and the normalised conditions.

Tensile specimens were manufactured to the dimensions shown in Fig. 3.5. As in the case of CT specimens, the gauge length of each specimen was polished to 1μm diamond paste level.

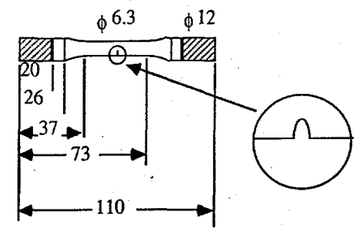

Figure 3.4 - Tensile specimen dimensions (all lengths are in mm). Notch in specimen that underwent LCF deformation is produced by a 2mm diameter mill and is 2mm deep.

In order to identify the load and strain at which the transition from elastic to plastic regime takes place, a tensile test was conducted for each material. Based on this information, the low cycle fatigue and high cycle fatigue applied amplitudes were chosen.

The low cycle fatigue applied amplitude chosen for 316L- Batch B was strain controlled with tensile strain ranging from 0.5-1.5% at 5Hz. The other materials were subjected to a variety of low cycle fatigue applied amplitudes. These different applied amplitudes are marked on the resulting plots. The high cycle fatigue regime chosen was a load-controlled applied amplitude of 1-9 kN at 5 Hz. Some results reported below refer to a load-controlled applied amplitude of 1-10 kN at 5 Hz, but they were obtained only for one series of high cycle fatigue tests.

After a selected number of low cycle fatigue cycles, the LCF exposure was stopped and a notch was machined into the middle of the tensile specimen, Fig. 3.5. This notch was produced by a 2 mm diameter mill and was 2 mm deep. This was done to concentrate the effects of the subsequent high cycle fatigue applied amplitude in a specific area of the specimen. This was done because in the CT specimen, HCF was concentrated by a notch and this was wanted to be duplicated for the tensile specimens. The notch depth and radius were kept constant for all tests. The high cycle fatigue applied amplitude was then applied to the specimens. The high cycle fatigue life (the number of cycles to failure) was recorded for specimens with different low cycle fatigue histories.

A fractional life summation was then carried out. In the present case, the following equation results:

$$C = \frac{n_{LCF}}{N_{LCF}} + \frac{n_{HCF}}{N_{HCF}} \qquad (3.1)$$

where n_{LCF} is the actual low cycle fatigue exposure (cycles),

N_{ICF} is the low cycle fatigue life,

n_{HCF} is the actual high cycle fatigue exposure (cycles), and

N_{HCF} is the high cycle fatigue life.

Fractional life summation was carried out for the combinations of low cycle fatigue and high cycle fatigue exposures. Plots of the fractional life sums as a function of low cycle fatigue exposure are presented in Section 4.2. Also presented are plots of the high cycle fatigue life as a function of the low cycle fatigue exposure.

3.4 Magnetic Moment Investigation

One possible mechanism for the fatigue life enhancement results for 316L stainless steel (Batch B) [122] might be associated with the formation of deformation induced martensite. The magnetic measurements were undertaken to determine the quantity of ferromagnetic material (ferrite and/or martensite) within the austenitic stainless steel in order to confirm or disprove this hypothesis. The literature shows a number of instances of this method being used [123, 124].

The three specimens that exhibited the greatest high cycle fatigue life enhancement were chosen. Namely, the magnetisation kinetics in the specimens that had been subjected to 0.5-1.5% low cycle fatigue at a frequency of 5 Hz for 250 cycles (that had then shown an increase in high cycle fatigue life of about 3 times, cf. Section 4.2) were measured. Three millimetre thick slices of material from within the gauge and thread sections were prepared using a Struers Accutom 2. Cutting was undertaken with a blade velocity of 700 rpm and a feed pressure of 0.4 bar.

The material for magnetisation measurements was taken from each specimen in two different locations in order to isolate the effects of low cycle fatigue exposure. The material from the threaded section of the specimen would not have been exposed to low cycle fatigue as this material was held within the grips of the Instron servohydraulic testing machine. The slice of material taken from the gauge length was removed approximately 5mm away from the machined notch. The material removed from the gauge length would have been exposed to low cycle fatigue, but not to substantial levels of high cycle fatigue. This is because the specimen had been notched prior to high cycle fatigue loading. Since the notch, introduced prior to HCF, concentrates the effects of high cycle fatigue in the material directly in front of it, the material from the gauge length will not have been exposed to high cycle fatigue. Visual observation of the deformation of the gauge length during low cycle fatigue indicated that uniform deformation was occurring.

From the 3mm thick disks cut, 3mm diameter cylinders were prepared by ultrasonic cutting. A Gatan model 601 ultrasonic disc cutter was used for this purpose. A cylinder was removed from the centre of a disc to avoid any possible edge effects. The cylinder was ultrasonically cleaned for 5 minutes in methanol and weighed in a Sartorius BA210S. Magnetic measurements were then conducted by a Vibrating Specimen Magnetometer (VSM); Aerosonic 3001, coupled with an Oxford Instruments 5T

Superconducting Solenoid. The magnetic moment of the disc, M, normalised by its mass, was plotted as a function of the magnetic field, H.

The intercept of the hysteresis curve with the M-axis (ie. the remanent magnetic moment) was determined and compared with the known saturation magnetisation of martensite.

Chapter Four: Results

4.1 Fatigue Crack Growth Investigations

4.1.1 Crack length data

Figure 4.1 displays crack length as a function of number of fatigue cycles for all tests done in the two series of experiments. Both the overload and non-overload fatigue tests are presented. The magnitude and duration of the overload are indicated. Only post overload data is shown. For the non-overload tests, data is shown from the same crack length as shown for the overload tests. Note that curves A-G are for the testing for the first specimen from each group.

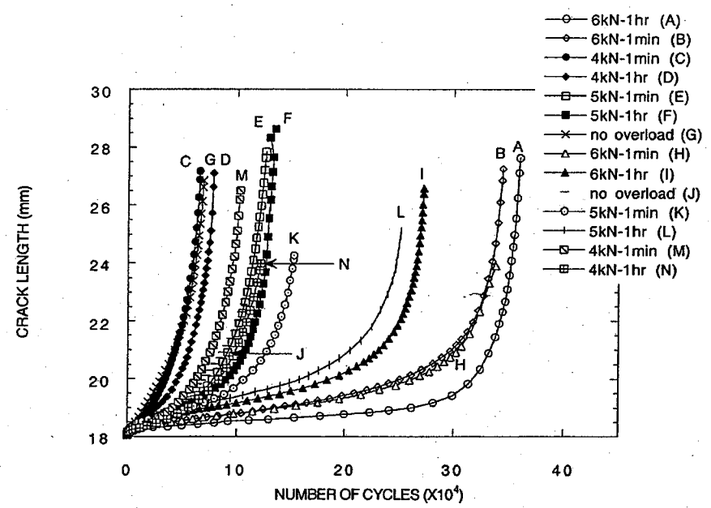

Figure 4.1 - Crack retardation behaviour for 316L stainless steel.

Transient acceleration was observed qualitatively in initial experiments. The acceleration could only be observed if no averaging of the data was carried out. These non-averaged results are presented in Fig. 4.2.

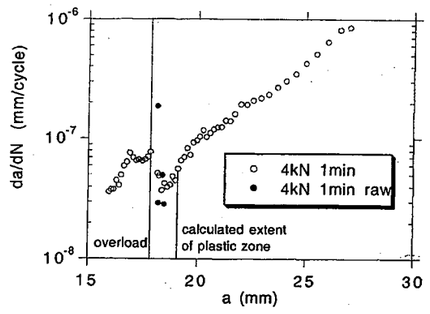

(a)

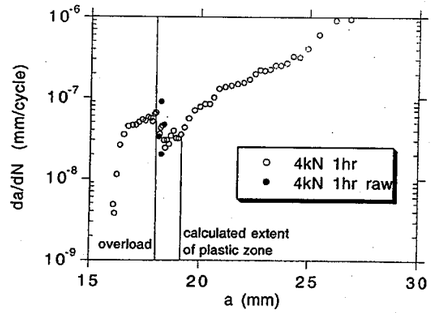

(b)

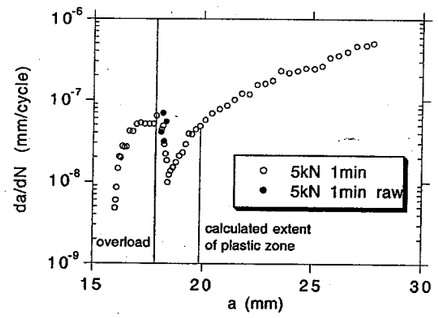

(c)

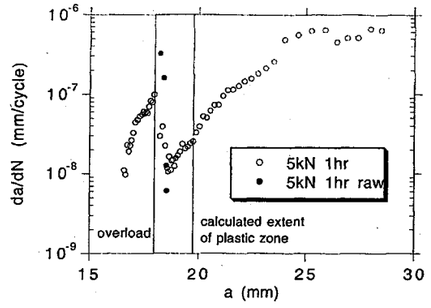

(d)

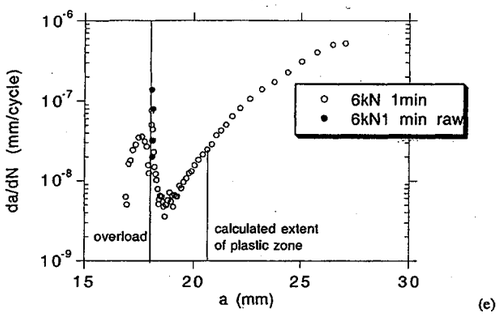

(e)

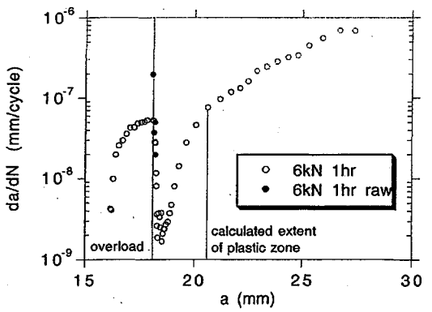

(f)

Figure 4.2 - Raw data points (full circles) plotted along with averaged data (open circles) to show initial acceleration of fatigue crack growth following overload for first group of tests of 316L (Batch A). The details of overloads are given in each diagram, (a) to (f). These plots correspond to Fig. 4.1, curves (A) - (G).

Additional tests with extra emphasis on initial crack growth following overload were also carried out. The results are presented in Fig. 4.3.

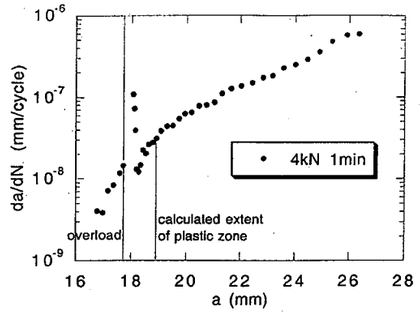

(a)

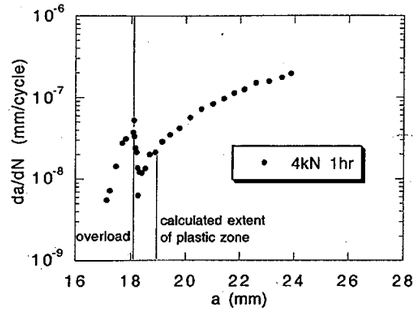

(b)

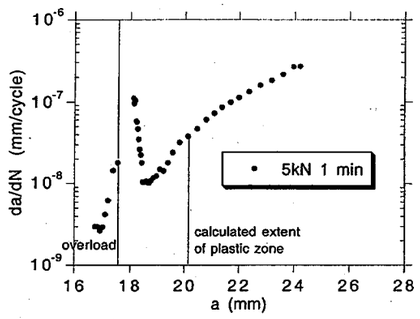

(c)

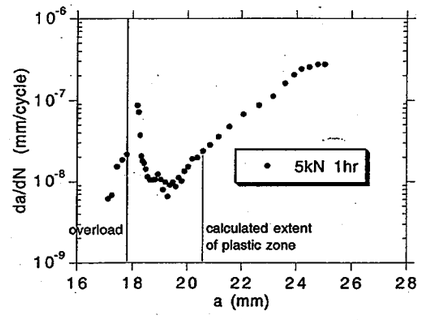

(d)

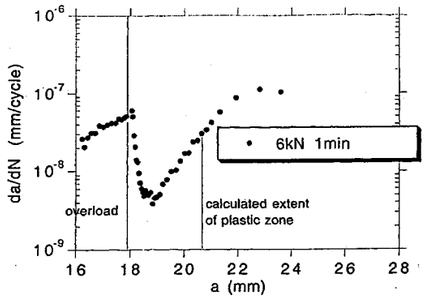

(e)

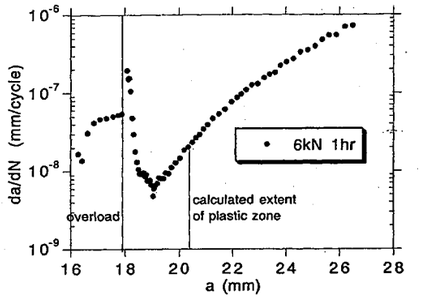

(f)

Figure 4.3 - Acceleration of fatigue crack growth following overload for additional tests of 316L stainless steel (Batch A). The details of the overloads are indicated above each individual diagram, (a) to (f). These plots correspond to Fig. 4.1, curves (H) - (N).

Figure 4.4 summarises the crack length at which the maximum, minimum and recovered fatigue crack growth rate observed. The figures in the legend indicate the amount of overload (kN) and its duration (minutes).

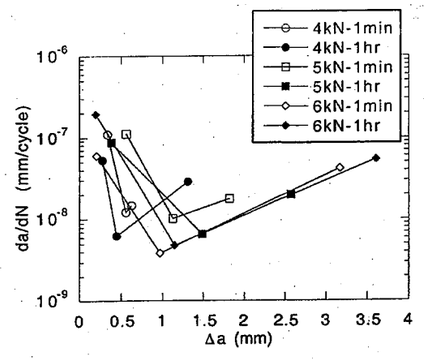

Figure 4.4 - Summary of minimum, maximum and recovered growth rates associated with tensile overloads for 316L stainless steel (Batch A).

4.1.2 Compliance Measurements

Prior to overload, the compliance curve is as shown in Fig. 4.5.

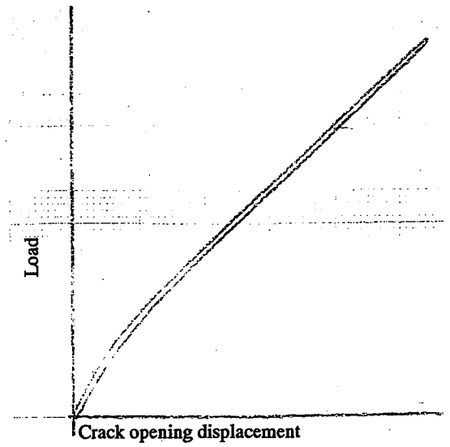

Figure 4.5 - Compliance curve in the absence of an overload for 316L (Batch A).

If the compliance data are plotted as a function of the crack length at which the compliance was measured, the following plot is found, cf. Fig. 4.6.

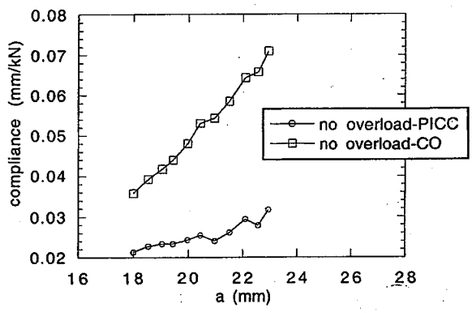

Figure 4.6 - Compliance of non-overloaded specimens as a function of crack length

316L stainless steel (Batch A).

If the compliance values for the specimens that were subjected to a low level of overload are plotted as a function of crack length, the following plot results, cf. Fig. 4.7.

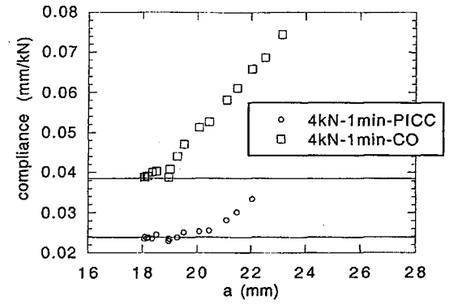

Figure 4.7 - Low overload compliance as a function of crack length

(316L steel – Batch A).

For specimens that were exposed to medium level overloads (e.g. 90%Pc for 1 hr and 115%Pc for 1 min), the plots are initially similar to that for a low overload. However, after the fatigue crack grows to a certain length, a second bend in the plot is noted, cf. Fig. 4.8. This is Discontinuous Crack Closure (DCC).

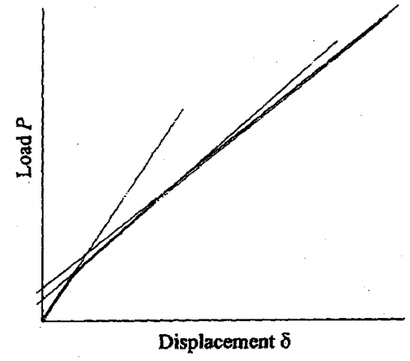

Figure 4.8 - Medium overload compliance curve after some fatigue crack growth

(316L stainless steel, 5kN-1min overload, Δa = 3.1mm).

The dependence of the compliance on the crack length in the three regimes is shown in Fig. 4.9 for two different overloading conditions: (a) 4kN, 1hr and (b) 5kN, 1min

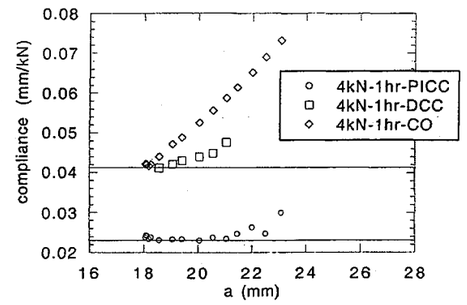

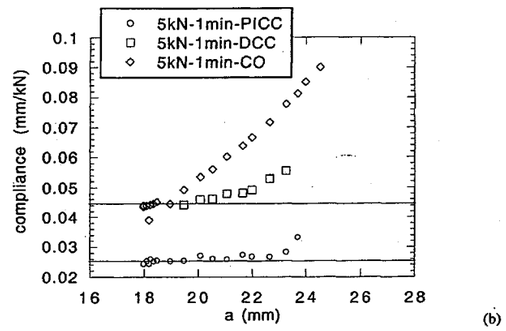

Figure 4.9 - Medium overload compliance as a function of crack length

(316L stainless steel – Batch A).

In the high level overload cases, crack closure is removed entirely, cf. Fig. 4.13. However, the discontinuous crack closure curve corresponding to the plateau section of the crack opening curve is still observed. The dependence of compliance on crack length is presented in Fig. 4.10.

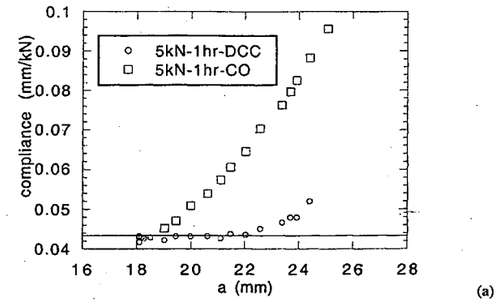

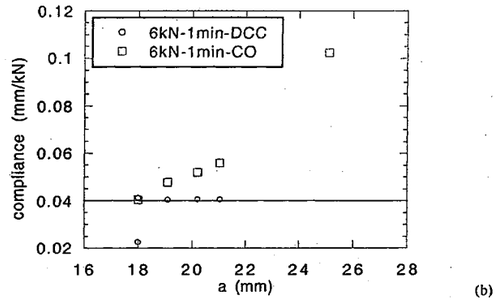

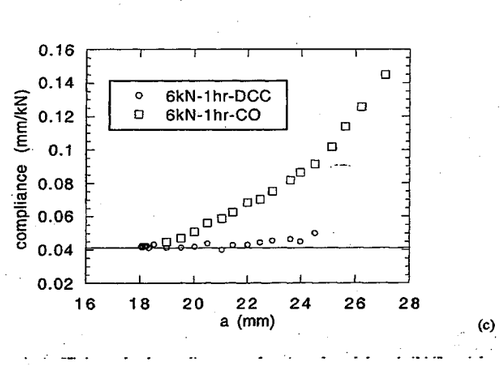

Figure 4.10 - High overload compliance as a function of crack length

(316L stainless steel – Batch A), (a) 5kN, 1hr; (b) 6kN, 1min; (c) 6kN, 1hr.

The compliance vs. crack length data for all tests is presented in Fig. 4.11.

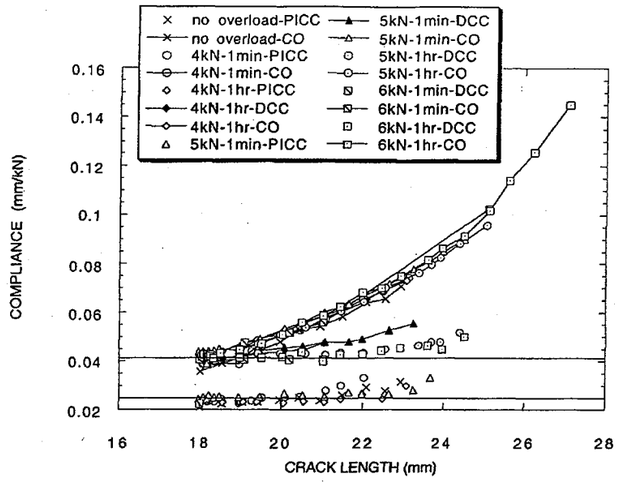

Figure 4.11 - Summary of compliance data for all overload tests

(316L stainless steel – Batch A).

4.1.3 Bend in a Compliance Curve

Figure 4.12 presents the load at which bends in the compliance curve appear as a function of the crack length. These bends separate the linear sections of the compliance curve and therefore separate the compliance measurements associated with PICC and DCC and crack opening.

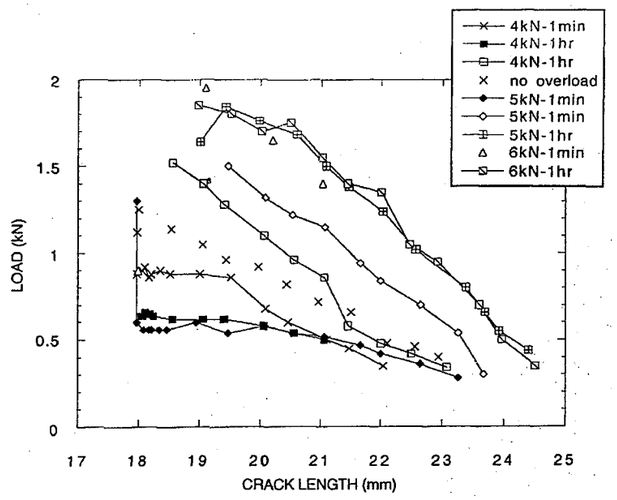

Figure 4.12 - Loads corresponding to bends in the compliance curves

(316L stainless Steel – Batch A).

4.1.4 Hysteresis

Figure 4.13 (a) presents an actual compliance plot for a high level overload case. The compliance plot was taken immediately following overload. Figure 4.13 (b) presents a schematic representation of the compliance curve.

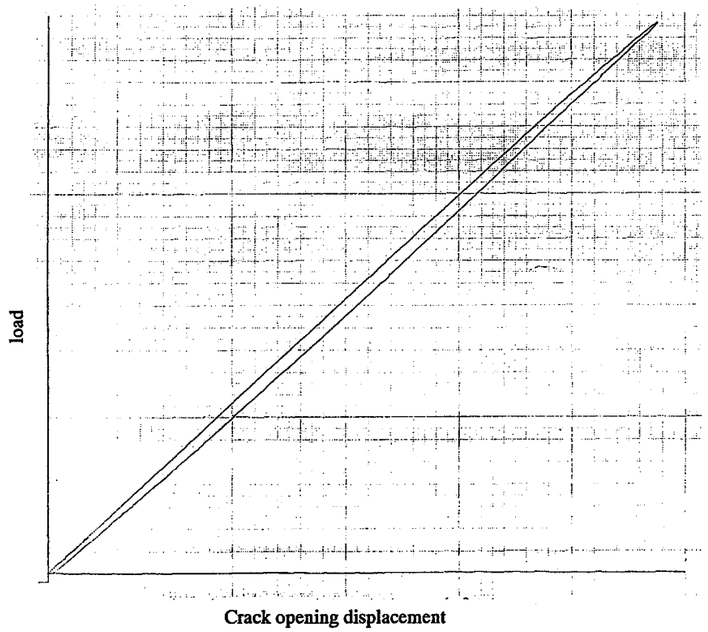

(a)

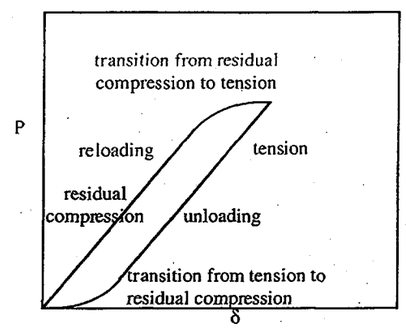

(b)

Figure 4.13 - Compliance curve following overload (316L stainless steel – Batch A, 5kN-1hour overload, 0.1-5kN compliance measurement taken directly after overload). (a) as observed (b) schematic.

4.1.5 Phi function

The plot in Fig. 4.14 shows the results of processing the compliance values of all the tests by the Phi function. The value of the Phi function is plotted versus the crack length at which the compliance measurement was taken.

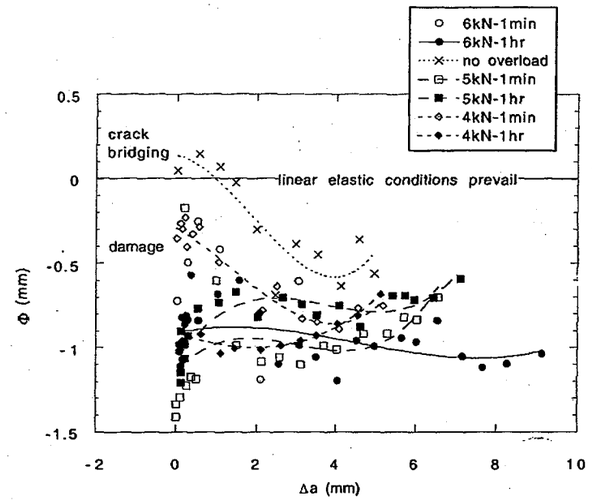

Figure 4.14 - Phi function plotted as a function of crack length increment Δa (316L stainless steel – Batch A).

4.1.6 Micrographs

4.1.6.1 Unperturbed cracks

The micrographs presented below refer to the crack tip (Fig. 4.15) and of a zone in the wake of a crack (Fig 4.16) in a CT specimen that had not undergone any tensile overload. In both cases, the crack is progressing upward.

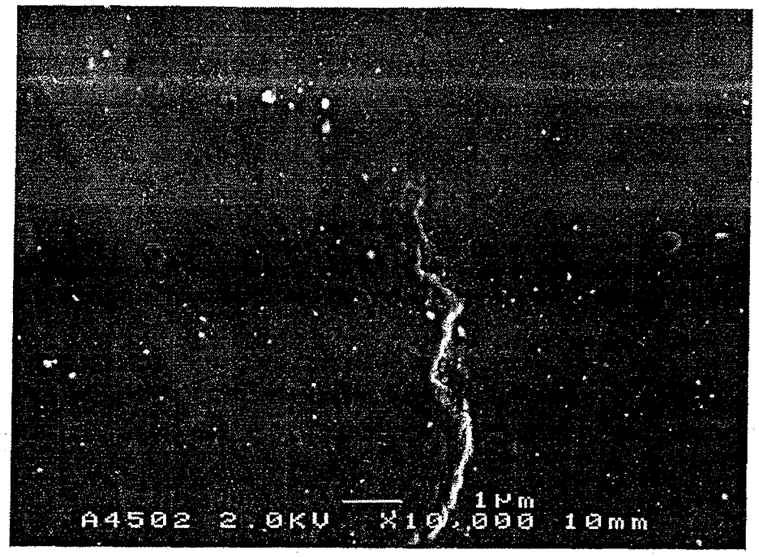

Figure 4.15 - Non-overloaded specimen's surface (fatigue crack profile) at the crack tip (316L stainless steel – Batch A) (crack growth to the top of the page).

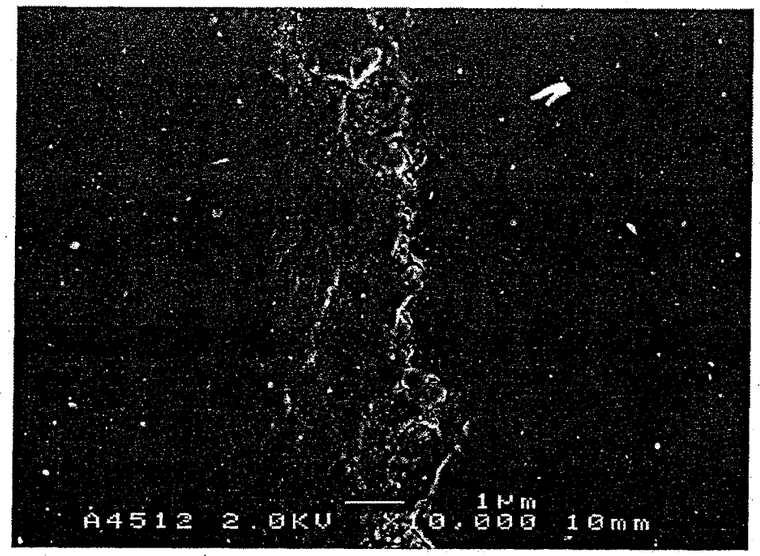

Figure 4.16 - Non-overloaded specimen's surface (fatigue crack profile) in the wake of a crack (316L stainless steel – Batch A) (crack growth to the top of the page).

The fracture surface of a non-overloaded specimen is presented in the FESEM pictures in Fig. 4.17. The areas of the fracture surface associated with fatigue (area A) and breaking open of the specimen (plastic tearing – area C) are marked. The smooth transition zone between areas A and C (area B) is associated with cleavage fracture through the FDZ.

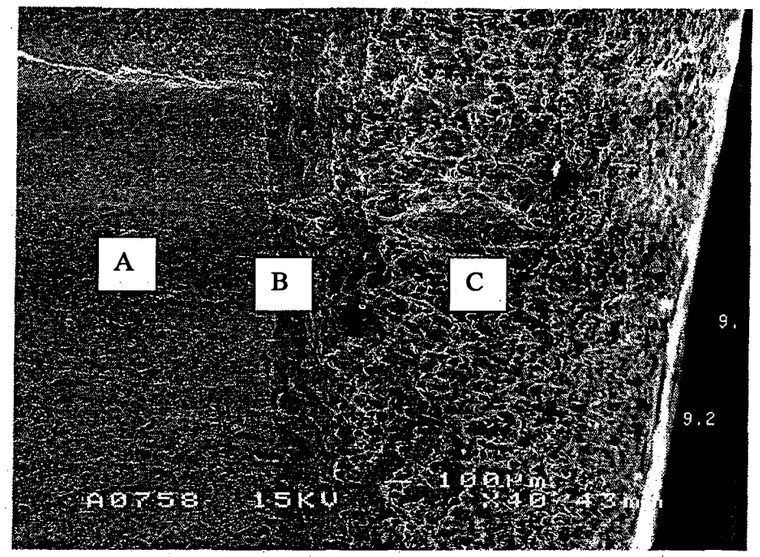

Figure 4.17 - Fracture surface of a non-overloaded specimen (316L stainless steel – Batch A) (crack growth to the right).

4.1.6.2 Tensile load less than P_C

Figure 4.18 shows the fracture surface of a fatigue specimen that underwent a tensile overload of 80% P_c The fracture surface associated with fatigue is shown in area A. The line seen at the A marker is where the 80% of PC overload occurred. The notch is seen in area C. The surface associated with tearing open of the specimen is area B. The fracture surface at the point of overload is enlarged in Fig. 4.19 (line A).

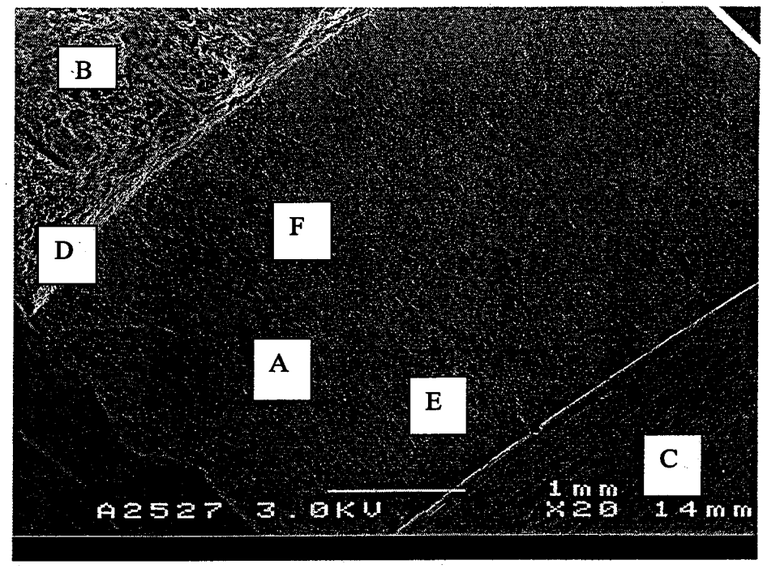

Figure 4.18 - Fracture surface of a fatigue specimen that underwent a tensile overload of 80% P_c (316L stainless steel– Batch A) (crack growth to the top of the page and to the left).

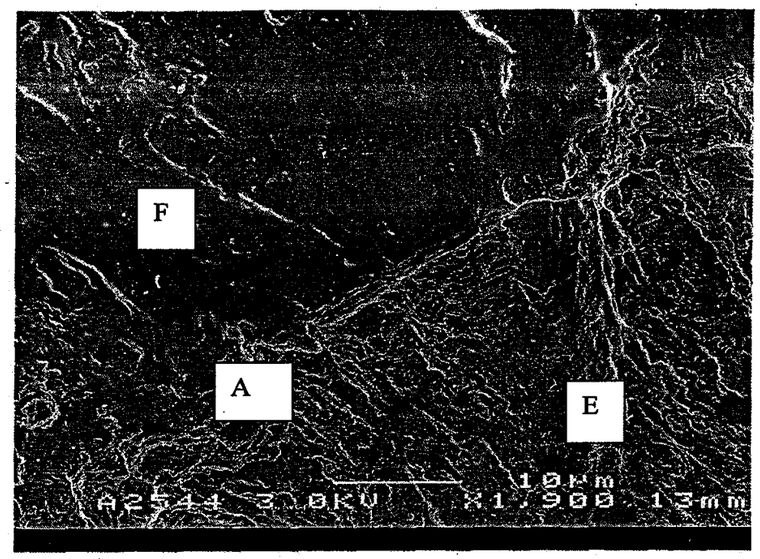

Figure 4.19 - Same as in Fig. 4.18, but with a larger magnification.

4.1.6.3 Tensile load greater than P_c

Figures 4.20 and 4.21 refer to fatigue specimens that were subjected to a tensile overload of 130% of P_C. Fatigue was not continued after the overload. The micrographs present views of the specimen surface (fracture profile).

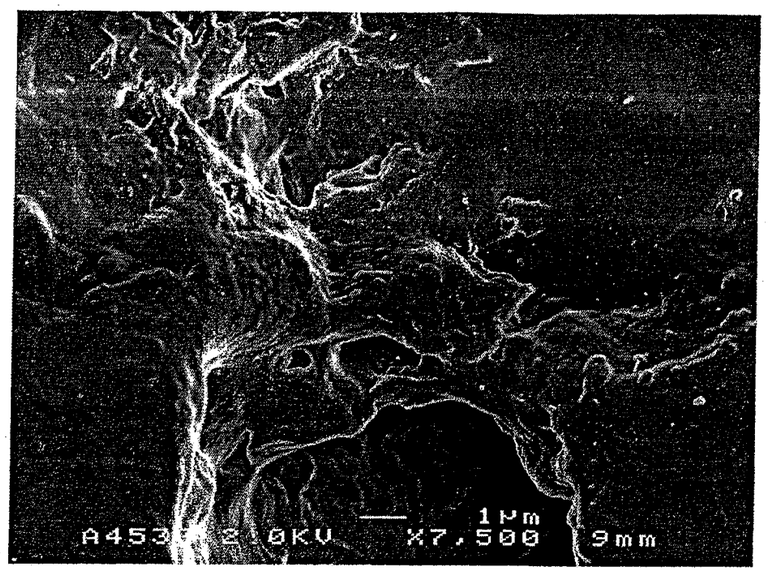

Figure 4.20 – Evidence of voids at crack tip after tensile overload (316L stainless steel– Batch A) (crack growth to the top of the page). The crack front is blunted due to the overload.

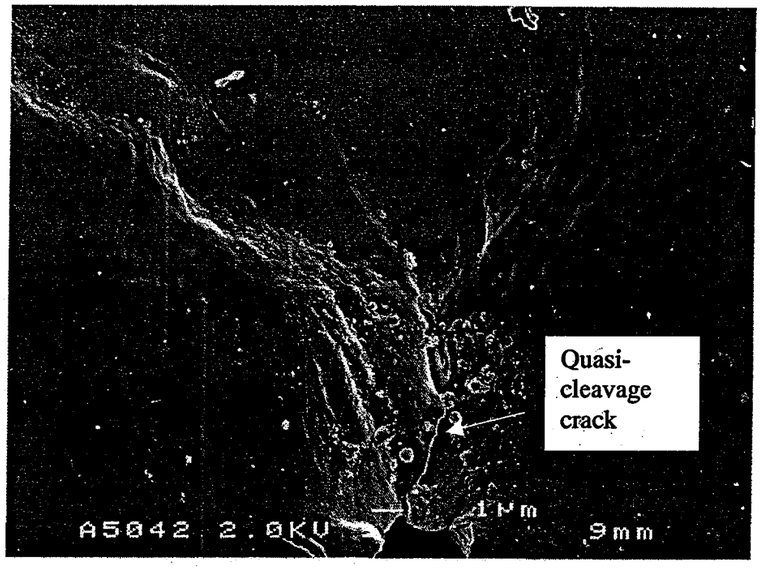

Figure 4.21 - Evidence of quasi-cleavage microcracking at crack tip after tensile overload (316L stainless steel– Batch A) (crack growth to the top of the page). The quasi-cleavage micro-cracking is seen as a white line ahead of the blunted crack tip.

In Figs. 4.22 and 4.23, the micrographs resulting from a 200% P_c tensile overload are presented. This specimen was subjected to fatigue after overload, but the cyclic load

was of an insufficient magnitude to cause further fatigue crack growth. Voids in Fig. 4.23 are readily observable in the zone between fatigue fracture surface and ductile tearing fracture surface.

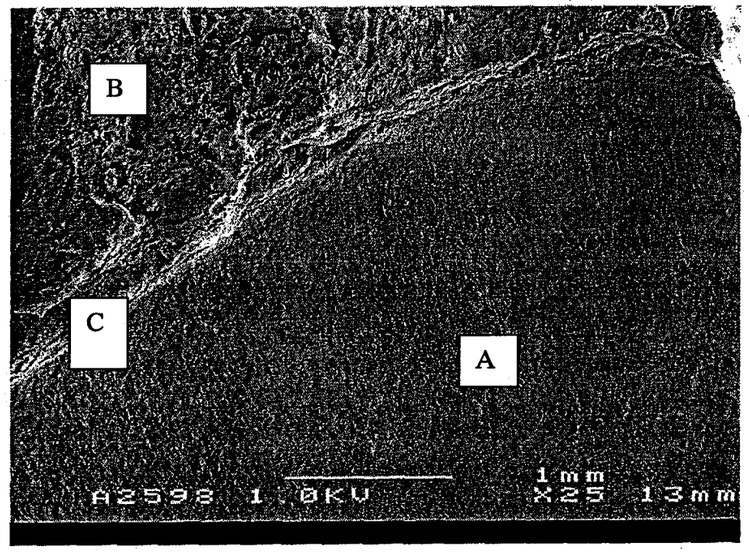

Figure 4.22 - Micrograph of a specimen that underwent a tensile overload of 200% PC (316L stainless steel– Batch A) (crack growth to the top of the page and left)).

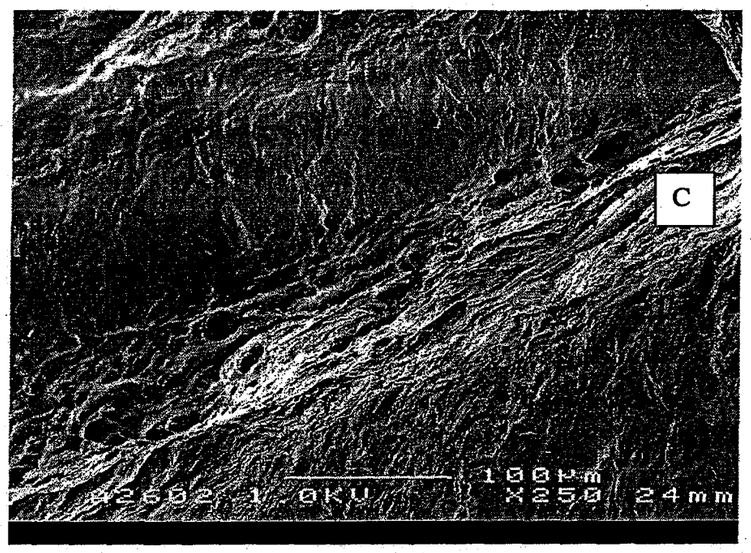

Figure 4.23 - Voids at crack tip on fracture surface. Smooth section on fracture surface indicates fracture to be a result of breaking open of specimen (316L stainless steel – Batch A) (crack growth to the top of the page and left)).

4.2 High Strain – Low Stress Interaction

4.2.1 316L Stainless Steel (Batch B)

The specimens produced from 316L (Batch B) were exposed to a low cycle fatigue applied amplitude that was strain controlled between 0.5-1.5 % at 5 Hz. The HCF waveform was a range of 1-9 kN at 5Hz. The results of testing 316L (Batch B) are presented in Fig. 4.24.

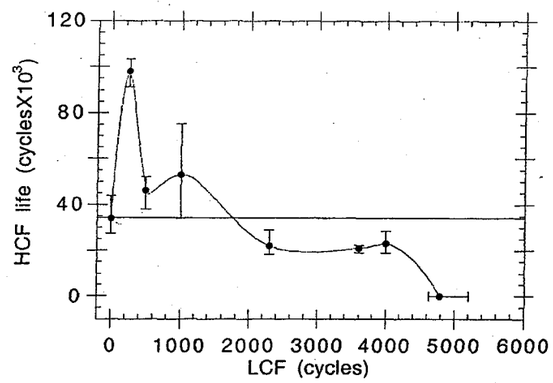

Figure 4.24 - High cycle fatigue life as a function of prior low cycle fatigue exposure (316L stainless steel – Batch B).

The horizontal line in Fig. 4.24 and in all further HCF life vs. LCF exposure plots presented below marks the 'virgin' HCF life, i.e. that of specimens that had not been LCF pre-loaded.

The fractional life summation for 316L (Batch B) is presented in Fig. 4.25 where the fractional life sum C is plotted as a function of the LCF cycle number.

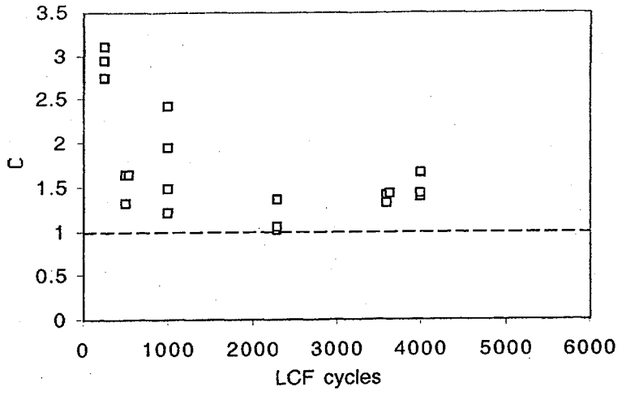

Figure 4.25 - Fractional fatigue life sum C as a function of prior low cycle fatigue exposure (316L stainless steel – Batch B).

4.2.2 316L Stainless Steel (Batch C)

Figure 4.26 presents the HCF life as a function of the LCF exposure. The strain ranges used in the LCF loading of the specimens are given in the insert. Frequency was 5Hz in all LCF tests and 20Hz in all HCF tests.

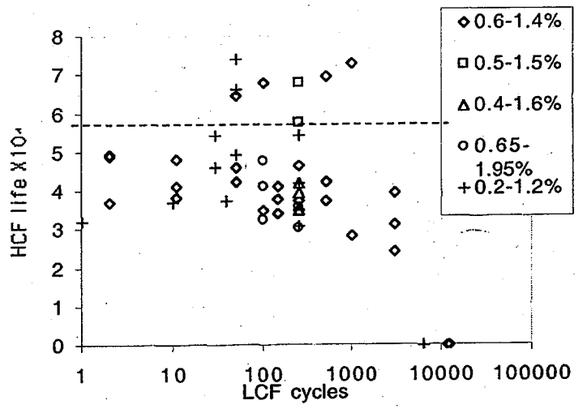

Figure 4.26 - High cycle fatigue life as a function of prior low cycle fatigue exposure (316L stainless steel – Batch C).

Figure 4.27 presents the normalised HCF life as a function of the normalised LCF exposure.

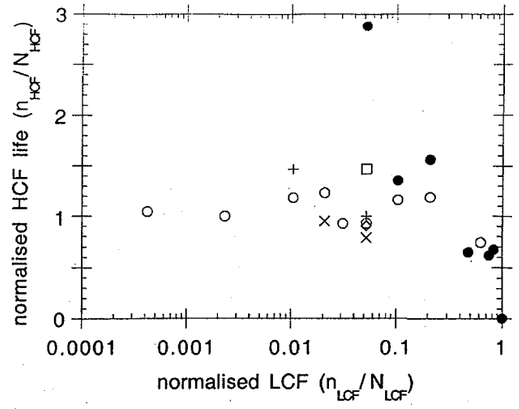

Figure 4.27 - Effect of the number of LCF cycles and the applied amplitude on HCF life (316L). The normalised HCF life is defined as the HCF life following LCF pre-straining divided by the virgin specimen's HCF life. Full circles refer to 316L (Batch B): (•: 0.5-1.5%, 5 Hz). The other symbols refer to 316L (Batch C). Open circles: (O : 0.6-1.4%, 5 Hz). Open squares : (n : 0.5-1.5%, 5 Hz). Open diamonds : (O : 0.4- 1.6%, 5 Hz). Xs : (X : 0.65-1.95%, 5 Hz). Crosses : (+ : 0.2-1.2%, 5 Hz).

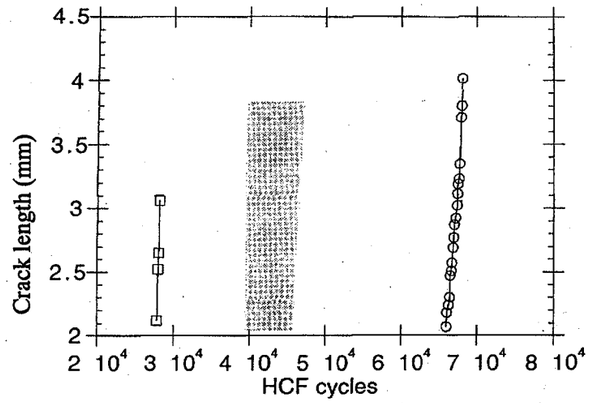

Figure 4.28 - Crack length vs. HCF cycle number for 316L (batch C).

The fatigue crack growth for 316L (batch C) is presented in Fig. 4.28.

4.2.3 Mild Steel (C1020)

This material was chosen as there was some concern that the life enhancement observed in 316L on both tensile specimens and CT specimens might be a result of a martensitic

transformation. Mild steel was thus tested to rule out a martensitic transformation. The next plots presented are for the mild steel C1020.

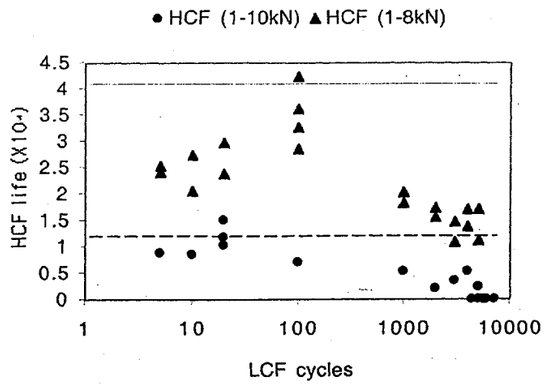

Figure 4.29 - High cycle fatigue life as a function of prior low cycle fatigue exposure for steel C1020.

As for 316L plots, the horizontal lines represent the reference ('virgin') high cycle fatigue life.

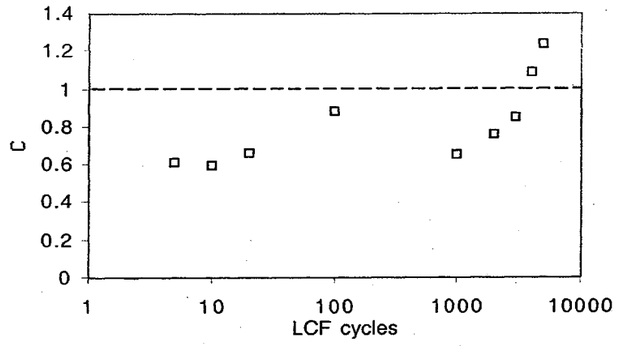

Figure 4.30 - Fractional life sum as a function of prior low cycle fatigue exposure for steel C1020 (HCF load range: l-8kN).

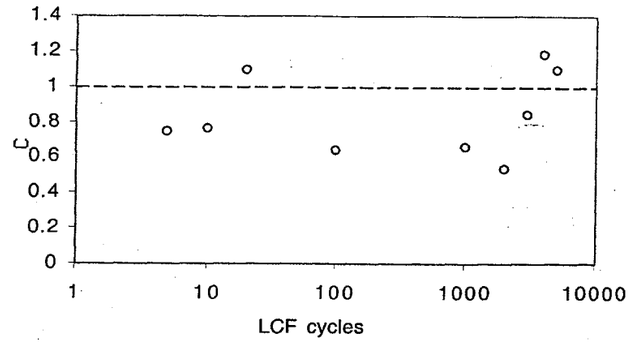

Figure 4.31 - Fractional life sum as a function of prior low cycle fatigue exposure for steel C1020 (HCF load range: 1-lOkN).

4.2.4 Mild Steel (AS1214)

The next material investigated was mild steel AS1214. The results for the material tested in the as-received condition and the normalised condition are shown in Figs. 4.32 & 4.33 and 4.34 & 4.35, respectively.

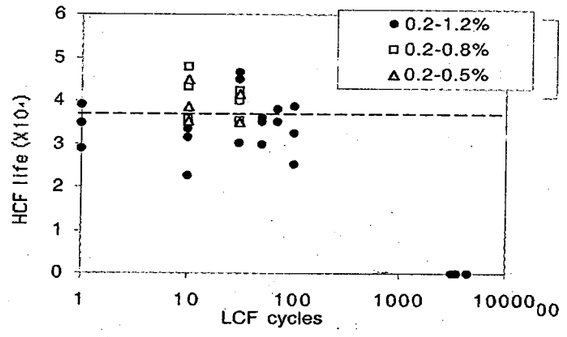

Figure 4.32 - High cycle fatigue life as a function of prior low cycle fatigue exposure for AS 1214, as-received.

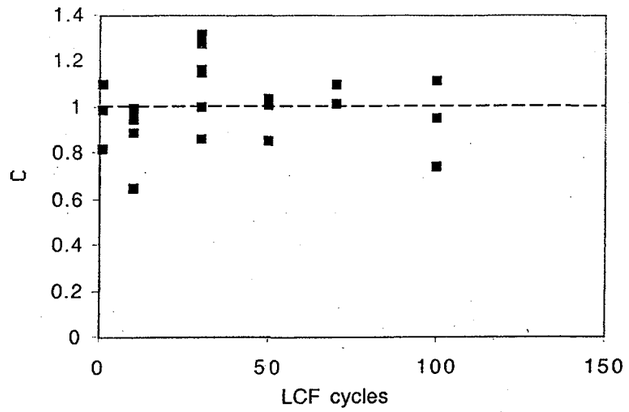

Figure 4.33 - Fractional life sum as a function of prior low cycle fatigue exposure (AS 1214, as-received).

4.2.5 Normalised Mild Steel (AS1214)

The tests were repeated with normalised material. The first question investigated for this material was whether even a singular tensile excursion beyond the yield point would affect the fatigue life (Fig. 4.34).

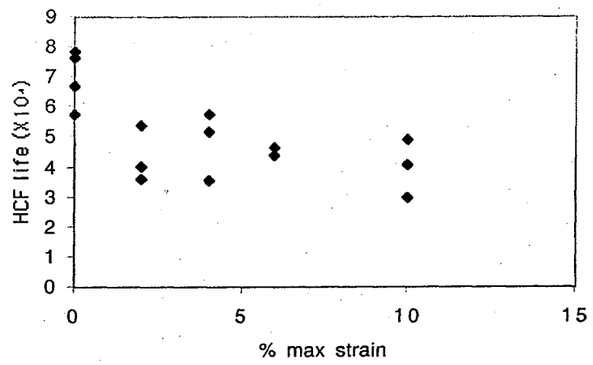

Figure 4.34 - High cycle fatigue life as a function of tensile strain in a singular overload (AS 1214, normalised).

Figures 4.35 and 4.36 present the HCF life as a function of the LCF exposure and the damage sum as a function of the LCF exposure, respectively.

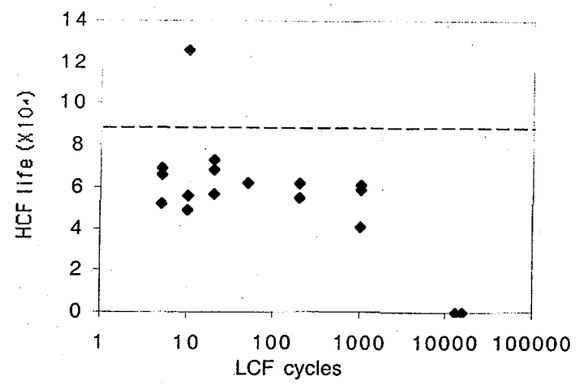

Figure 4.35 - High cycle fatigue life as a function of prior low cycle fatigue exposure (AS 1214, normalised).

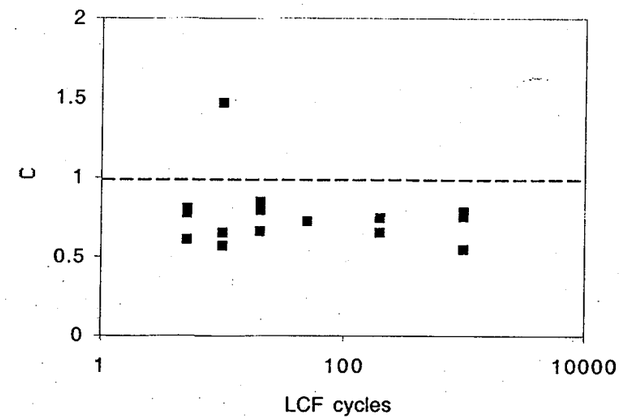

Figure 4.36 - Sum of fractional fatigue lives as a function of prior low cycle fatigue exposure (AS 1214, normalised).

4.2.6 Aluminium alloy 6060-T5

In order to see whether the violations of Miner's rule observed on steels also occur in non-ferrous alloys, an aluminium alloy (6060-T5) was tested in a similar fashion. Figure 4.37 shows the dependence of HCF life of the alloy on the LCF cycle number. The attendant fractional life summation plot is shown in Fig. 4.38.

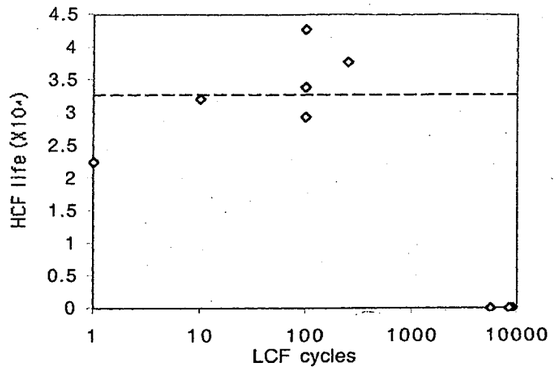

Figure 4.37 - High cycle fatigue life as a function of prior low cycle fatigue exposure for aluminium alloy 6060-T5.

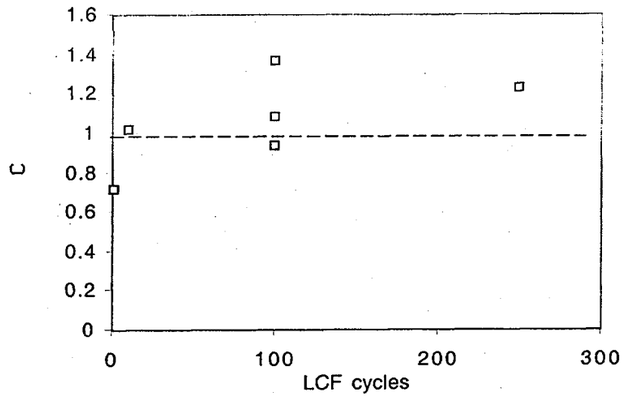

Figure 4.38 - Fractional life sum as a function of prior low cycle fatigue exposure for aluminium alloy 6060-T5.

4.3 Magnetic Moment Investigation

While no LCF induced martensitic transformation can occur in the mild steel and aluminium tested, it cannot be ruled out for the 316L steel. Magnetic measurements were therefore conducted in order to see whether a martensitic transformation in the 316L stainless steel could be considered responsible for the observed fatigue life extension.

The hysteresis loop was taken three successive times to ensure that saturation of the magnetisation behaviour had occurred. The diagram presented in Fig. 4.39

demonstrates that saturation had occurred within the first loop. The three loops measured are seen to coincide exactly. Despite this, the third hysteresis loop was used for all subsequent calculations.

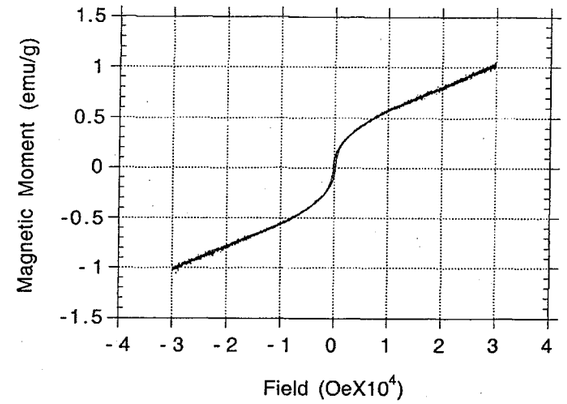

(a)

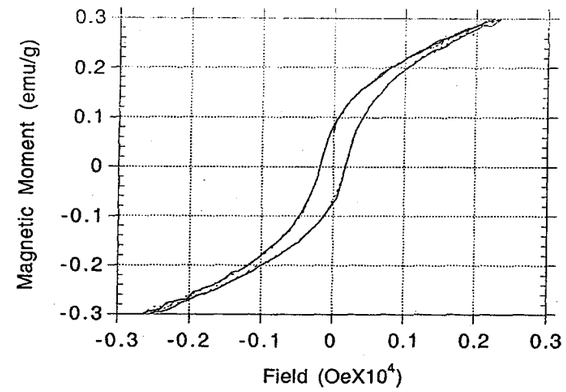

(b)

Figure 4.39 - Three successive hysteresis loops of the gauge section of specimen 1. Three loops ensure saturation of the specimen. The coincidental loops indicate that the specimen was saturated on the first loop. (316L stainless steel (Batch B) - tensile specimens that showed greatest increase in HCF life (cf. Fig. 4.32).

Figure 4.40 presents the saturated hysteresis loops for each particular specimen.

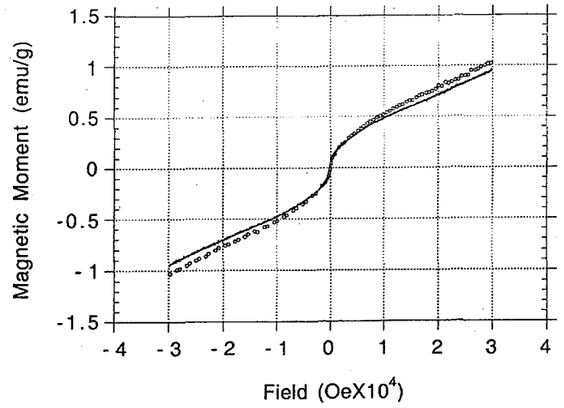

(a)

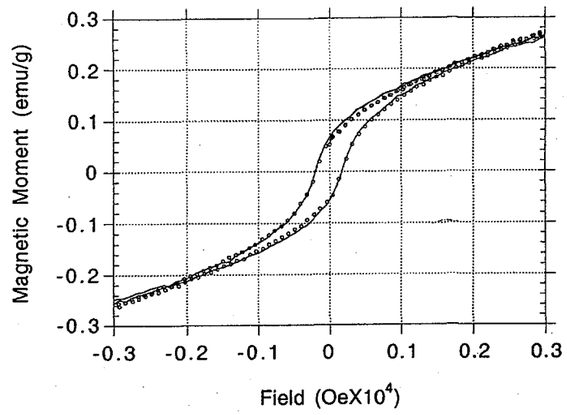

(b)

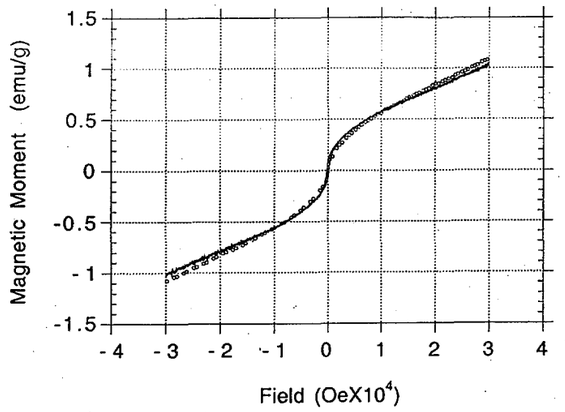

(c)

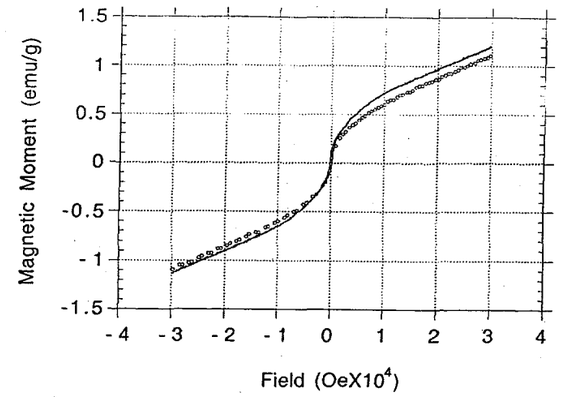

(e)

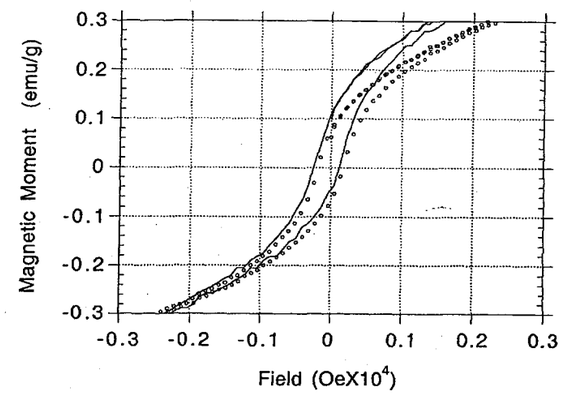

(f)

Figure 4.40 - Normalised magnetic moment plotted as a function of magnetic field (316L – Batch B). Dotted lines correspond to material from threaded section of specimen while solid lines refer to material from gauge section, (a) specimen 1 (b) enlargement (c) specimen 2 (d) enlargement (e) specimen 3 (f) enlargement

Chapter Five: Discussion

5.1 Fatigue Crack Growth Investigations

5.1.1 Crack length data

Despite all tests of Fig. 4.1 displaying a retardation of fatigue crack growth following the tensile overload, a sizeable scatter exists. The scatter varies from 10-30%, with one exception of a data scatter of 50% for one test. However, this should be tempered with the fact that fatigue results are notorious for data scatter – hence the common use of double logarithmic plots for Paris plots. Analysis of Fig. 4.1 suggests that the amount of retardation is related to both the magnitude and the duration of the overload.

In addition, presentation of the above data in a fatigue crack growth rate vs. crack length plot shows that there is a transient acceleration in fatigue crack growth immediately following the overload. The literature includes work into retardation of fatigue crack growth following a single tensile overload [72, 73], particularly by Ward-Close [74], Dauskardt [75, 76], Suresh [28], Ritchie [77, 78] and Hou [79]. Damri and Knott [30], Tsukuda [57] and Skorupa [80] have also reported transient crack growth acceleration. It can be seen in both Fig. 4.2 and Fig. 4.3 that the first data points following overload show an increase in da/dN. Subsequently, the fatigue crack growth rate decreases to a value lower than that observed prior to overload. After reaching a minimum, the crack growth rate gradually increases with the crack length, passing its pre-overload level and eventually outgrowing it as failure approaches. The acceleration of the crack growth occurs over the first 300 μm or so of crack tip propagation following the overload. The crack tip displacement over which deceleration prevails is one order of magnitude larger. Fatigue crack growth reaches pre-overload levels after the crack tip has travelled about 7-8 mm.

Two vertical lines can be seen in Fig. 4.2 and 4.3. The first one marks the crack length at which the tensile overload occurred, the second indicates the size of the plastic zone resulting from the tensile overload. The size of the plastic zone was calculated via the Wheeler equation [81]. Wheeler postulated that the fatigue crack growth rate should recover to pre-overload levels after the plastic zone was passed through. As can be seen from the plots, the fatigue crack growth rate has approximately regained its pre-overload level (recovered) when the crack tip has traversed the plastic zone, as calculated by the Wheeler equation.

In Fig. 4.4 it can be seen that the fatigue crack growth rate reaches a maximum after about 300 μm of crack growth, following the tensile overload. This is consistent for all the tensile overload tests. The magnitude of the maximum fatigue crack growth rate varied from test to test. No consistent relationship between the maximum fatigue crack growth rate and magnitude of tensile overload was found. The crack length at which the minimum fatigue crack growth rate occurs varies greatly between specimens. Generally, the greater was the magnitude or duration of overload, the greater was the crack length that had to be grown through to reach the minimum fatigue crack growth rate. The crack length at which fatigue crack growth recovers is related in a similar way to the level of tensile overload.

5.1.2 Compliance Measurements

The typical compliance plot that results from a non-overloaded specimen is presented in Fig. 4.5. The compliance calculated from the lower section of the two slope plot was similar to that of the material without a fatigue crack. This is consistent with the idea that the fatigue crack is closed when low loads are applied due to plasticity-induced crack closure. The compliance calculated from the upper slope relates to the remaining material ligament and the crack tip conditions.

As the fatigue crack grew, compliance measurements were taken at regular intervals. Figure 4.6 shows the change in compliance as the fatigue crack grew. It can be seen that the crack opening compliance values increase with crack length. This is an obvious result as the specimen's remaining ligament is steadily decreasing. The lower compliance curve corresponds to that of the lower section of Fig. 4.5. This indicates that for small crack length, the lower part of the compliance curve corresponds to that of an uncracked specimen. However, as the crack grows, the compliance increases until this section disappears. In essence, the PICC is slowly disappearing as the ligament of remaining

material decreases. This would be the result of the ligament being less able to exert elastic stress to close the fatigue crack.

Figure 4.7 presents the change in compliance for a low overload specimen (e.g. 90%Pc for 1 min). The compliance plots show a two-slope curve similar to that for non-overloaded specimens, cf. Fig. 4.5, despite the overload. An overload would blunt the crack to some degree. The result of blunting the crack is to lessen the plasticity induced crack closure resulting from fatigue crack growth prior to overload. What can also be observed are the plateau sections of both the plasticity induced crack closure and crack opening curves. Horizontal lines in the plot highlight these plateau sections. The plateaus exist for a period of crack growth and then the compliance values increase in a similar manner to those of the non-overloaded specimen. The existence of the plateaus implies that even though the crack is growing as a result of fatigue loading, the compliance remains unchanged, presumably as a result of residual compression that causes the post-overload fatigue fracture surfaces to come into contact. After the crack has grown enough to lessen the effect of the overload induced residual compression, the compliance of the specimen increases in a manner similar to that of the non-overloaded specimen.

Figure 4.8 shows an as-observed plot of the compliance for a medium level overloaded specimen. Similar to the low overload test, plasticity induced crack closure is observed. This is indicative of the overload resulting in crack blunting, but not of an order sufficient to fully remove plasticity induced crack closure caused by pre-overload fatigue crack growth. Figure 4.8 differs from the low overload test in that three distinct linear sections are evident. Figure 4.9 shows that the discontinuous crack closure curve extends from the plateau section of the crack opening curve.

For the specimens under large overload (e.g. 115%Pc for 1 hr, 130%Pc for 1 min and 130%Pc for 1 hr, cf. Fig. 4.10), the post-overload compliance curves degenerate to a single straight line. This indicates that plasticity induced crack closure stemming from pre-overload fatigue crack growth has been removed completely as a result of crack tip blunting.

Figure 4.11 shows the compliance measurements as a function of crack length for all the specimens. The compliance measurements for PICC, DCC and crack opening show distinct groupings, despite the different levels of overload. The crack opening compliance is a function of the material only and therefore is easily understandable. The crack opening compliances also show the highest degree of grouping. Both PICC and DCC groupings are slightly less

concentrated. The PICC and DCC groupings show that both PICC and DCC maintain their plateau levels longer the higher the overload was. This is obvious as the level of PICC and DCC are larger for larger tensile overloads.

5.1.3 Bend in Compliance Curve

In addition to the compliance value associated with each linear section of the compliance plot, the load at which the bends occur gives important information. This tells us what load is required to separate the fracture surfaces that are in contact due to plasticity induced crack closure or discontinuous crack closure. Figure 4.12 shows the variation in the elbow of the compliance curves as a function of crack length.

When no tensile overload is applied, the level of PICC is not altered. The load to separate the fatigue fracture faces steadily decreases with crack length. This is the result of the ligament of material steadily being reduced. This material can therefore exert less elastic stress on the fatigue crack to close it.

For low and medium level overloads, there is an initial drop in the load required to separate the fatigue fracture surfaces. This corresponds to a reduction in the PICC that existed prior to the tensile overload. The PICC is reduced by crack blunting. Apparently, the overload was not sufficient to fully blunt the crack tip, but some blunting occurred so that less load is required to separate the fatigue fracture surfaces. This load remains nearly constant until it starts to drop off at roughly the same rate as for the non-overloaded specimens.

The high level overload specimens have the PICC (as a result of fatigue crack growth) totally removed by the overload. After some crack growth PICC associated with the new crack growth appears. The load required to separate the new fatigue fracture surfaces that are produced following the overload can also be seen in Fig. 4.12. It is high due to the residual compressive forces in action as a result of the tensile overload. However, it drops off as crack growth proceeds.

5.1.4 Hysteresis

The compliance measurement is limited in its application. If continued to high loads, it is a destructive test as the material is overloaded. During fatigue crack growth, one is limited to compliance measurements that do not exceed the maximum load associated

with the applied fatigue amplitude. In the tests conducted, this was followed except for the conditions after a tensile overload. After an overload, the compliance could be measured to the maximum load applied during the overload. The compliance was measured in 1 kN intervals. For instance, for an overload of 6kN, compliance measurements were taken over the ranges of 0.1 kN-3.0 kN, 0.1 kN-4.0 kN, 0.1 kN-5.0 kN and 0.1 kN-6.0 kN. A hysteresis was noted as demonstrated in Fig. 4.13.

The observed plot as seen in Fig. 4.13(a) has been schematically represented in Fig. 4.13(b). As explained above, the material at the fatigue crack tip is experiencing plastic deformation. This is due to the high stress concentration at the crack tip. The rest of the material is deformed elastically. It is the change in the material at the crack tip that causes the hysteresis. As the external load changes, the residual stress on the material at the crack tip is altered. A schematic of this process can be seen in Fig. 4.13(b). When the external load increases, a linear section of the plot is- observed, as the material is fully under residual compression. A transitional period then occurs as the residual compression reduces to zero and the material at the crack tip experiences tensile forces.

The compliance associated with the two linear sections schematically shown in Fig. 4.13(b) was measured and the two values were found to be identical. It was also found that these values were equal to the crack-opening compliance in the non-overloaded specimen. This suggests that the compliance measurement is insensitive to the strain hardening that occurs during an overload. This is consistent with the results of a direct tensile test.

5.1.5 Phi function

An insight into the crack tip conditions is provided by compliance measurements. The compliance measurement combines information regarding both the crack tip conditions and the crack length. By processing the compliance measurements via the Phi function [32], the dependence of the compliance upon the crack length is removed. The information thus extracted concerns the crack tip conditions only. If $Cco(a) = C(a)$, then $\Phi = 0$ and the ideal elastic situation is recovered. If $Cco(a) < C(a)$, then $\Phi > 0$ representing the situation where crack-wake bridging (e.g. due to fracture surface roughness) is the dominant influence. Finally, if $Cco(a) > C(a)$, $\Phi < 0$ implying that the fatigue damage (e.g. due to micro-cracking or void formation) in front of the crack tip is the dominant factor.

Figure 4.14 shows an overall negative trend for Φ. This signifies damage ahead of the

crack tip. An increase in duration or magnitude of tensile overload results in an increasingly negative Φ value, implying that an increase in magnitude and/or duration of tensile overload causes an increase in the damage ahead of the crack tip. As fatigue crack growth occurs after the tensile overload, the Φ value approaches that of the test not perturbed by an overload. This is an indication that the damage ahead of the crack tip, characteristic of the unperturbed test, is restored.

5.1.6 Micrographs

5.1.6.1 Unperturbed Cracks

In Fig. 4.15, the surface is featureless away from the crack tip. At the crack, however, undulations in the specimen surface are visible. This observation suggests the presence of plastic deformation. As the fatigue crack grows, it seeks out any local weaknesses to progress through. These weaknesses include grain boundaries, voids, slip systems, etc. The asperities thus produced are what enables contact between the two sides of the crack during plasticity-induced crack closure. Even in a non-overloaded specimen, the plastic deformation associated with crack growth at the tip results in plasticity-induced crack closure. The gaps produced between the asperities as a result of plasticity induced crack closure (Fig. 4.16) should be noted.

Despite the low global loading placed on the specimen, the sharp fatigue crack tip produces a high stress concentration which results in the material ahead of the crack tip being subjected to a load exceeding the material's yield strength. The repeated plastic deformation of the material ahead of the crack tip produces damage (just as in low cycle fatigue). The damage is often in the form of voids. As fatigue loading continues, necking in ligaments between voids occurs leading to crack growth. The zone of damage ahead of the crack tip is referred to as the 'fatigue crack process zone'.

In Fig. 4.17, although generally flat, the fatigue fracture surface (area A) does display the undulations that appear in the profile micrographs (Fig. 4.16 and 4.17). No striations were observed, as is often the case in steels. Figure 4.17 also shows the fracture surface associated with breaking open of the specimen (area C). Notice the difference to the relatively flat fracture surface associated with fatigue (area A). The fracture surface caused by opening the specimen is much rougher due to the gross plastic deformation involved. Fatigue causes plastic deformation ahead of the crack tip but at a small scale. Gross yielding causes large-scale plastic deformation that is easily observed by the naked

eye. Between the fatigue fracture surface and the fracture surface caused by breaking open the specimen, there is a smooth region (area B). As discussed above, the material ahead of the crack tip contains damage as a result of the fatigue loading and the sharp fatigue crack tip. The presence of the smooth fracture area immediately ahead of the fatigue fracture surface suggests that when the specimen was broken open, shear fracture took place through the material containing damage. The fracture surface is therefore smooth and shiny. It can be conjectured that the thickness of the smooth region can be used to assess the size of the damage zone.

5.1.6.2 Tensile load less than P_C

The micrographs in Figs. 4.18 and 4.19 show a specimen that underwent loading of 80% of P_c after fatigue deformation. In this case the specimen was fatigued after the overload. Figure 4.18 clearly shows the demarcation point where the overload occurred (line A). The fracture surface as a result of tearing open of the specimen can be seen in the upper left of Fig. 4.18 (area B). The notch can be seen in the lower right part of the picture (area C). The fatigue surface is quite smooth. The fatigue surface before and after overload are indicated by areas E and F.

At high magnification, the fatigue fracture surface can be seen in the lower right part of Figure 4.19 (area E). Striations are absent; the fracture surface immediately ahead of the fatigue surface is smooth, as in previous micrographs (area A). This would suggest the shear through this material occurred in this case as well. However, this specimen was subjected to fatigue following overload, while the previous specimen was just broken open. This suggests that the crack progressed rapidly through the material, in a manner similar to shear, despite the loading regime being high cycle fatigue. This is consistent with the mechanical observations of the previous section where an accelerated crack growth was observed following an overload.

5.1.6.3 Tensile load greater than P_C

Both voids (Fig. 4.20) and quasi-cleavage microcracking (Fig. 4.21) are observed ahead of the blunted crack. The tensile load applied blunts the fatigue crack tip. Still, damage occurs ahead of the crack tip. Since the tensile overload could not have caused the damage, merely have enhanced it, this suggests that the damage existed prior to the tensile overload. Note that the previous micrographs of non-overloaded crack tip did not

show these damage characteristics. It is suggested that the voids are too small to be visualised unless a tensile overload enhances the damage in the fatigue damage zone. The voids in the above figures are largest near the crack tip. The void size is inversely related to the distance from the crack tip. Micro or quasi-cleavage cracking [30] is seen in Fig. 4.21. The distance from the crack tip at which either quasi-cleavage cracks or voids are seen is an order of magnitude smaller than the distance over which acceleration occurs. Literature suggests that the size of the damage zone is many times greater in the interior of the specimen [30], while the above micrographs were taken at the specimen surface.

Figure 4.22 shows the fatigue surface filling most of the micrograph (area A). The upper left of the figure shows the fracture surface caused by breaking open of the specimen (area B). Again, a rougher area follows a smooth zone (area C). Figure 4.23 shows this zone immediately ahead of the fatigue fracture surface with a greater magnification (area C). Voids are observed ahead of the smooth zone. The voids are similar in both position and size to those seen in Fig. 4.20.

In these figures we see all the aspects of the crack progression. The flat fatigue surface can be seen initially. As apparent in the figures, fatigue crack growth cannot occur after the high tensile load. This is seen as a result of residual compression and strain hardening of the material ahead of the crack tip following overload. The size of this zone and the magnitude of the compressive stress depend on the magnitude of the overload and the material's condition. If the overload is of such a magnitude that the residual compressive stress is greater than the stress applied during the subsequent fatigue applied amplitude, no fatigue crack growth will occur, as the material at the crack tip would not experience any tensile stress. Following opening of the specimen, the smooth surface is a result of shear fracture through the material contained within the fatigue damage zone. The voids are visible reminders of the damage contained within the fatigue damage zone being enhanced by tensile loading. As the specimen is broken open, i.e. the crack front has to pass through the material outside of the fatigue damage zone where the material is undamaged, global plastic yielding must occur resulting in a ductile tearing fracture surface.

An overload less than P_c does not enhance damage present in the fatigue damage zone and so voids are not visible. However, the damage is still there and when the specimen is broken open, shear occurs as documented by a smooth section. An overload in excess of

P_C enhances the damage and both voids and a shear fracture surface are observed when the specimen is broken open.

5.2 *High Strain – Low Stress Interactions*

5.2.1 316L Stainless Steel (Batch B)

The following trend can be observed in Fig. 4.24. The HCF life of virgin 316L stainless steel shows some scatter (see error bar), the average life being about 35,000 cycles. After 250 low cycle fatigue cycles with 0.5-1.5%, 5Hz applied amplitude, the high cycle fatigue life increases to approximately 100,000 cycles. This observation shows that the prior LCF exposure caused the HCF life to nearly treble. With more low cycle fatigue exposure, the high cycle fatigue life drops from the peak high cycle fatigue life of 100,000 to a plateau-like region of approximately 23,000 cycles. Here the LCF exposure does not affect the subsequent HCF life. This plateau region sets in after about 1000 LCF cycles. It represents a 30% drop in HCF life from that of the non LCF pre-loaded specimens and an 80% drop from the peak HCF life. Low cycle fatigue failure occurs after about 5,000 cycles (which is an average over three LCF-only tests).

Figure 4.25 shows the damage summation, C, as a function of LCF pre-treatment. Henceforth, a horizontal dashed line in the summation plots corresponds to C = 1. This is the theoretical linear cumulative fractional life sum according to Miner's rule and that used in ASTM standards. The fractional life C has been calculated in accordance with Eq. 3.1.

The fractional life sum for the combination of high cycle fatigue and low cycle fatigue exposure in 316L (Batch B) is greater than 1 in all instances. This suggests that the overall fatigue life has been extended by the prior low cycle fatigue exposure. The greatest degree of life extension occurs at lower numbers of LCF cycles. As described above, a plateau was observed in the HCF life vs. LCF exposure plot. Even though the level of this plateau is below the HCF life of virgin specimens, the fractional life summation plot of Fig. 4.25 indicates that the combination of high cycle fatigue and low cycle fatigue exposure still results in an overall life extension.

4.2.2 316L Stainless Steel (Batch C)

Different suppliers provided the batches of 316L. Although the batches are of the same nominal type, differences in chemical and mechanical properties exist. Analysis of data for 316L (Batch C) in Figs. 4.26 and 4.27 suggest that little enhancement of the HCF life occurs with any of the prior LCF exposure. There are some data points above the dashed line that corresponds to the average HCF life without prior LCF exposure. However, the amount of life enhancement does not match the spectacular result obtained with 316L (Batch B). Also, the number of instances of high cycle fatigue life extension is less than for 316L (Batch B).

The fatigue crack growth for 316L (batch C) is presented in Fig. 4.28. The shaded region refers to the area of plot occupied by non-LCF trained specimens (ie. normal range of HCF crack growth). Open circles refer to a specimen that has experienced 100 cycles of LCF (0.6-1.4% at 5Hz) prior to HCF. Crack initiation, as characterised by the high cycle number, is retarded. Crack growth, as characterised by the slope of the graph, is also retarded. Open squares refer to a specimen that has experienced 1000 cycles of LCF (0.6-1.4% at 5Hz) prior to HCF (crack initiation enhanced).

The effect is significantly larger than the scatter between individual specimens that had not been exposed to LCF pre-training (shaded region). This suggests that suitable LCF exposure results in a retardation of HCF crack initiation. Furthermore, a decrease in the slope of the curve, i.e. in the fatigue crack growth rate, is also observed. These findings confirm previous results [82] and provide qualitative evidence that training of the material by LCF exposure in a suitable regime leads to a delay in crack initiation and also to a decrease in the fatigue crack growth rate under subsequent HCF deformation.

4.2.3 Mild Steel (C1020)

Figure 4.29 shows that high cycle fatigue life initially drops for small numbers of LCF cycles. HCF life increases lightly around 100 LCF cycles and then drops off again. This behaviour, seen for two types of applied amplitude (l-8kN and 1-lOkN), was commonly observed, regardless of HCF applied amplitude.

In the fractional life summation plots, Figs. 4.30 and 4.31, an initial drop in C is observed. The magnitude of C approaches or even surpasses 1 for large LCF cycle numbers, but the average is generally below unity. This demonstrates that for this material and the present combination of low cycle fatigue and high cycle fatigue,

Miner's rule is violated, as was the case for 316L. However, unlike for 316L, an overall decrease in fatigue life is observed.

4.2.4 Mild Steel (AS1214)

Figure 4.32 shows that there is little change in the HCF life with small numbers of LCF exposure. This is also evident in Fig. 4.33 where the damage summation also hovers around unity.

4.2.5 Normalised Mild Steel (AS1214)

As Fig. 4.34 illustrates, a tensile excursion to the indicated levels of strain causes a substantial drop in HCF life. The magnitude of the tensile strain does not affect the HCF life, however. The lack of effect of pre-straining upon the HCF life has been observed in the literature [83].

The effect of low cycle fatigue on subsequent high cycle fatigue life is presented in Fig. 4.35. In this case, no extension of high cycle fatigue life could be achieved. A similar conclusion follows from the fractional life summation in Fig. 4.36.

This material also seems to disobey Miner's rule. For this material and the particular combination of LCF and HCF used, the overall fatigue life was reduced.

4.2.6 Aluminium Alloy 6060-T5

Generally, the HCF life does not change significantly with exposure to low cycle fatigue from that of the virgin material's HCF life. Similarly, C does not significantly depart from unity. This suggests that this material, when exposed to this combination of low cycle fatigue and high cycle fatigue, obeys Miner's rule with reasonable accuracy. However, deviations of up to 40% observed need to be considered in design with this Al alloy.

5.3 Magnetic Moment Investigations

As can be seen in Fig. 4.40, there is little difference between the material that was exposed to low cycle fatigue and the material that was not. The plots show behaviour

that is largely paramagnetic, ferromagnetism related hysteresis behaviour being not significant. However, even in the material that had not been exposed to low cycle fatigue, a hysteresis loop and a non-zero remanence were observed. This indicates that some ferromagnetic material, either martensite and/or residual ferrite, was present. The volume fraction of ferromagnetic material can be estimated by dividing the measured saturation magnetisation by that of martensite (approximately 146 emu/g [84]). The estimate shows that the amount of ferritic material in all specimens is less than 0.5%. The saturation magnetisation in the gauge length of each specimen was approximately the same as in the corresponding threaded section.

These facts demonstrate that LCF exposure has not resulted in any martensitic transformation of the austenitic 316L material and that the observed life enhancement cannot be attributed to LCF induced martensitic transformation.

Chapter Six Conclusions

6.1 Fatigue Crack Growth Investigations

1. Fatigue crack growth occurs by a process of damage accumulation in the material in front of the crack tip.

The existence of the fatigue damage zone within the plastic zone is a topic of some controversy. However, it is consistent with the idea that fatigue cracks grow via repeated plastic deformation at the crack tip that causes crack extension cycle-by-cycle. At the peak load during the fatigue loading, plastic deformation will be at a maximum of its activity. When the minimum load of the fatigue applied amplitude is reached, residual compression will occur. This is repeated until damage nucleates in a fatigue damage zone that is enclosed within the larger plastic zone.

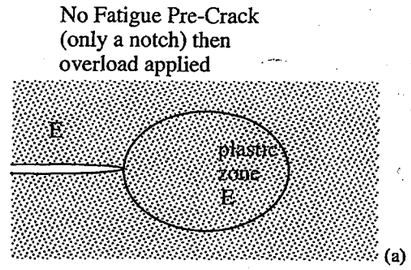

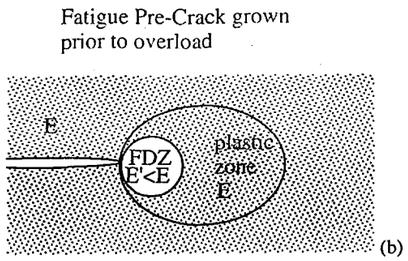

Figure 6.1 - Key difference between overload in a notched specimen (a) and in a specimen with a fatigue crack (b), ie. the presence of a fatigue damage zone (FDZ). E and E' denote the elastic modulus in the undamaged and damaged material, respectively.

The damage increases until the crack can grow through the damaged material, which locally has reduced fracture toughness. In effect, the local Young's modulus is reduced from that of the material. This was observed where Φ values dropped below zero, cf. Fig. 4.14. A fatigue crack grows by advancement of the crack tip through a localised damage zone that is continually produced. By this mechanism, fatigue crack growth occurs at fatigue loads below the fracture toughness of the material. Electron micrographs obtained in this study have shown the presence of fatigue damage ahead of the crack tip and in the wake of the crack during pure fatigue without overload, cf. Fig. 4.15, 4.16 and 4.17. The fracture surface was shown to be flat but irregular, with no striations formed, cf. Fig. 4.17. Observation of a broken open fatigue specimen documents the presence of smooth shear fracture through part of the specimen. This is observed in both non-overloaded and overloaded specimens, cf. Fig. 4.17, 4.19 and 4.22. Shear occurs through the weakened fatigue damage zone. The material ahead of the fatigue damage zone fails in a typical ductile fashion, cf. Fig. 4.17, 4.18 and 4.22. Tensile overloads above the critical load corresponding to the fracture toughness of the material cause the formation of voids and quasi-cleavage micro-cracks, cf. Fig. 4.20 and 4.21. Broken open specimens again show a shear fracture surface next to the regions where voids and micro-cracks are observed, cf. Fig. 4.22. The observations of a shear fracture surface support the notion of the fatigue damage zone ahead of the fatigue crack tip. The conclusions reached above are also supported by systematic compliance measurements that were made prior, during and after a tensile overload, cf. Fig. 4.5 – 4.12. Different crack opening stages are revealed during a single fatigue loading cycle, cf. Fig. 4.13. The negative values of the compliance function also confirm the existence of a fatigue damage zone, cf. Fig. 4.14. An additional conclusion to be made is that it may be incorrect to consider the stress intensity distribution about a fatigue crack tip to be only a function of

the applied load and the crack length. The effect of the fatigue damage zone requires special attention.

2 Tensile overload creates a plastic deformation zone ahead of the crack tip. The material within this zone is strain hardened and also causes PICC. It has been found that retardation of post-overload fatigue crack growth is mainly a result of the increased fatigue resistance of the strain-hardened material within the overload plastic zone.

The magnitude and duration of a tensile overload results in an overall retardation of fatigue crack growth, cf. Fig 4.1. Retardation occurs as the crack grows through the material within the plastic zone associated with the tensile overload. The data gathered correlates well with the Wheeler equation, cf. Fig. 4.2, 4.3 and 4.4. If an overload is sufficiently large, fatigue crack growth at pre-overload levels is halted. The crack opening compliance of the non-overloaded and overloaded specimens was found to be identical. This suggests that the compliance measurement is insensitive to the strain hardening that occurs during an overload, cf. Fig. 4.13. We conclude that retardation is associated with plasticity induced crack closure to a lesser extent. It is concluded that crack growth retardation is related to strain hardening. As the plastic zone is larger than the enhanced fatigue damage zone, the fatigue crack growth, after an initial acceleration, slows down dramatically when the crack tip leaves the damage zone, while still moving within the plastic zone. In addition to the strain hardening and residual compression, due to the rapid crack growth through the enhanced fatigue damage zone, there has not been enough time for the crack to create a new fatigue damage zone. This is supported by the observation that not all materials form striations [19]. For example, steels rarely exhibit striations [19]; rather, microvoid coalescence is seen at high ΔK levels [19].

The idea that strain hardening is the main cause of retardation [67] has been challenged by some researchers [29, 85]. The opposition to strain hardening as the retardation mechanism is based on three findings. Firstly, strain hardening should be at a maximum at the crack tip, due to the fact that the greatest stress concentration occurs there. This should mean that the fatigue crack growth rate should be at a minimum in this near crack tip region. Instead, as found in these and other experiments, a transient acceleration is observed immediately following an overload immediately following an overload. Hence, strain hardening was ruled out as a major factor of fatigue crack growth retardation. However, the presence of a fatigue damage zone is not recognised by the

authors [29] as a cause of fatigue crack growth. Secondly, simulating a plasticity induced crack closure as a result of tensile overload by filling the crack with epoxy resulted in crack growth retardation, without initial acceleration [29]. This provides support to the idea that retardation is caused by crack closure. However, it was not reported whether or not the entire crack was able to be force filled with epoxy [29]. Plasticity induced crack closure associated with an overload does not result in the entire surface contacting, so analysis is difficult. Thirdly, strain hardening was attempted to be observed via hardness testing of the specimen surface, at the crack tip. Unfortunately, the experiment was done on as-received material that would most likely have been rolled. In this case, microhardness measurement would not be appropriate due to surface effects. In any case, as the author concedes [29], a large scatter in the data was present.

3. **Fatigue cracks grow by a process of damage accumulation in the material ahead of the crack tip (FDZ). A tensile overload enhances the damage ahead of the crack tip. This results in a transient acceleration in the fatigue crack growth following overload.**

A tensile overload also causes a transient acceleration in fatigue crack growth, cf. Fig. 4.2 and 4.3. This increased fatigue crack growth occurs over the first 300μm or so of crack growth following an overload, cf. Fig. 4.4. This value varied little with level of tensile overload. This suggests that the period of acceleration is not related to the level of overload. Rather, it is related to the size of the FDZ, which is related to the fatigue loading conditions prior to overload. Results of processing of the compliance measurements by the Phi function indicate that increased tensile overload causes increased damage ahead of the fatigue crack tip, cf. Fig 4.14. Cleavage fracture is observed head of the crack tip of specimen subjected to fatigue, cf. Fig. 4.17. Voids or quasi-cleavage microcracks are observed ahead of the crack tip of an overloaded specimen, cf, Fig. 4.22 and 4.23. Voids are observable in the cleavage fracture zone of a grossly overloaded specimen, cf. Fig. 4.23. The size of the voids are related to the damage increase within the FDZ. The damage is introduced by fatigue, but expanded by tensile overload.

Figure 5.1 displays a set of typical compliance plots taken at certain crack lengths for 316L stainless steel (Batch A).

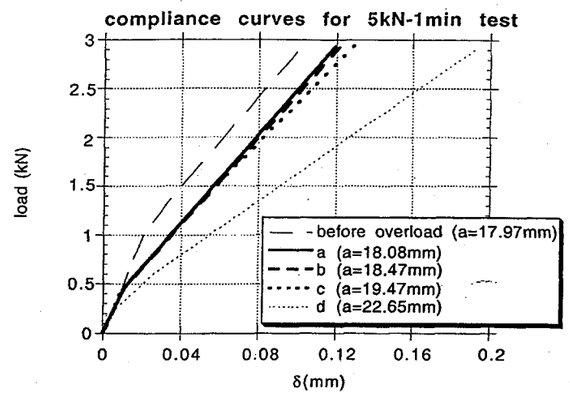

Figure 6.2 - Superimposed typical compliance plots recorded at different crack lengths (316L stainless steel – Batch A).

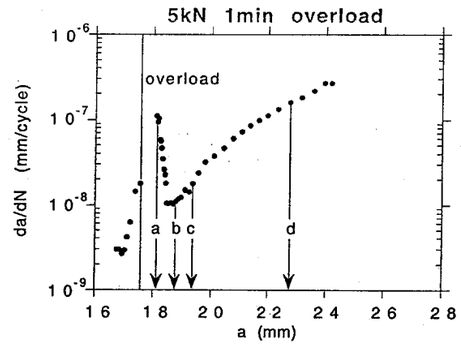

Figure 6.3 – Crack growth plot indicating points at which compliance plots in Fig. 6.1 were recorded (316L stainless steel – Batch A).

Prior to overload, plasticity induced crack closure is visible in the lower part of the figure and the transition to crack opening occurs at approximately 1.1 kN. Following overload, the load at which the fracture surfaces separate is much lower implying that crack blunting is responsible. However, the plasticity induced crack closure and crack opening compliance have not changed. Upon application of fatigue loading identical to that before overload, acceleration occurs followed by retardation. The compliance plots taken at the maximum and the minimum fatigue crack growth rates are almost identical. This is a clear indication that crack closure is not primarily responsible for this large change in fatigue crack growth rate. It is concluded that it is the fatigue damage zone, rather than removal of plasticity induced crack closure, that is responsible for the acceleration.

As outlined above, the high stress concentration in front of a fatigue crack tip exceeds the yield strength of the material in this local region inducing plastic deformation there. During fatigue, repeated plastic deformation of the material at the crack tip occurs leading to damage formation. This damage concentrates at the crack tip within a damage zone. In our picture the damage zone is enclosed within the plastic zone. The crack grows when the damage within the fatigue damage zone is high enough. When the crack grows, progressive yielding causes damage within the next small area of material and the crack continues to grow. Crack growth is accompanied with propagation of the damage zone along with the crack tip in a self-consistent way. Following overload, the damage within the damage zone is enhanced. For example, existing microvoids are further enlarged. When fatigue loading is re-applied, the crack travels faster through this zone of enhanced damage

6.2 *High Strain –Low Stress Investigations*

4. **316L Stainless Steel (Batch B) displayed an enhancement of fatigue life with LCF pre-training. Crack initiation and propagation was retarded in 316L (Batch C) by similar LCF pre-training. This behaviour was not observed in mild steel (C1020 and AS1214) or aluminium alloy (6060-T5). A martensitic strain induced transformation was found to be not responsible for the observed behaviour of 316L (Batch B). It is concluded that this behaviour supports the findings of fatigue crack growth experiments, i.e. that strain hardening is primarily responsible for fatigue crack growth retardation following tensile overload.**

Due to the evidence that crack closure was not a major contributor toward fatigue crack growth retardation, but rather that strain hardening and residual compression was, it was suggested that the material ahead of the crack tip may be thought of as experiencing low cycle fatigue, even though the overall specimen was under HCF loading regime. Different materials were investigated in order to assess the role of a possible LCF induced martensitic transformation in the large enhancement in high cycle fatigue life observed in 316L (Batch B). Aluminium and mild steels, if they demonstrate similar behaviour, would be exhibiting it for other reasons.

Low cycle fatigue can have a dramatic effect on the subsequent high cycle fatigue life. An interesting aspect is that the effect of the low cycle fatigue is highly dependent upon the

number of LCF cycles. For a relatively small numbers of cycles, around 250 for 316L (Batch B), an increase in the high cycle fatigue life is seen, but a decrease in the high cycle fatigue life was observed beyond a peak value.

A principle behind the traditional S-N testing approach is that exposure to fatigue causes an incremental, linear increase in damage to the material. The results obtained in this work and other reports [19] suggest that this conclusion is not followed in many instances. A striking observation on 316L (Batch B) was that low numbers of low cycle fatigue cycles could actually increase a material's resistance against high cycle fatigue.

The microstructural condition of the material, the low cycle fatigue applied amplitude and the number of LCF cycles applied all influence the subsequent high cycle fatigue life of a specimen. It was also observed that positioning the low cycle fatigue applied amplitude around the transition between elastic and plastic regimes has a significant impact upon the subsequent high cycle fatigue life extension.

In total, six different materials have been tested in this way. These include two types of 316L austenitic stainless steel (Batch B and C), two types of mild steel (one of these mild steels having been tested again after normalisation) as well as aluminium alloy 6060-T5. The 316L stainless steel (Batch B) returned results showing that, for certain conditions, the exposure of the material to low cycle fatigue causes an increase in the high cycle fatigue life. Tests on 316L (Batch C), the normalised AS 1214 and the as-received C1020 showed that the interaction of low and high cycle fatigue caused an increase of HCF life, but an overall reduction in fatigue life. The aluminium alloy 6060-T5 and as-received AS 1214 followed the traditional Palmgren-Miner rule, in that the interaction did not change the fatigue life, i.e. the fractional fatigue life sum at failure equalled unity.

For 316L (Batch C), the normalised AS1214 and the as-received C1020 the Palmgren-Miner rule is not followed. Moreover, the fractional life sum shows a drop in the fatigue life with small numbers of LCF cycles, but the fatigue life does recover if more low cycle fatigue exposure is allowed. Both 316L (Batch B and C) and the mild steels show improvement in fatigue properties with low cycle fatigue exposure, while in the case of aluminium alloy 6060-T5, only the virgin HCF life level is reached with increased number of LCF cycles. Magnetic measurements demonstrate that high cycle fatigue life enhancement is not due to LCF induced martensite transformation.

The effect of tensile overload on the fatigue crack growth rate in 316L stainless steel (Batch A) has lead to a picture in which the material directly ahead of the fatigue crack tip

can be thought of as experiencing low cycle fatigue even in nominally HCF regimes. Indeed, failure occurred in the fatigue damage zone after much less than 10,000 cycles of repetitive yielding. Further, the material within the FDZ experiences varying levels of LCF load, depending on distance from the crack tip and the attendant stress concentration. Since the fatigue damage zone can be seen as a set of elements experiencing varying degrees of low cycle fatigue, it was decided to apply varying numbers of LCF cycles to tensile specimens and then observe how this affected the subsequent high cycle fatigue life. Structures are normally subjected to high cycle fatigue, but it is postulated that the material at the crack tip is experiencing low cycle fatigue due to the stress concentration at the crack tip.

Appendix

Proof of Palmgren-Miner Linear Damage Accumulation Rule

It is assumed that on Stage II, crack growth is dominant at both high and low stress levels. Crack propagation law for Stage II.

$$\frac{da}{dN} = A\Delta\sigma^m a^q \qquad \text{(A1)}$$

Consider a crack growing from a_0 to a_1 at the first stress level and then growing from a_1 to a_2 at a second stress level. If failure then takes place, then $a_2 = a_f$ (final crack length).

From Eq. A1, $$\frac{da}{a^q} = A\Delta\sigma^m dN \qquad \text{(A2)}$$

Consider stressing at one level $\Delta\sigma_1$ from start to finish, then:

$$\int \frac{da}{a^q} = \left[\frac{a^{q+1}}{q+1}\right]_{a_0}^{a_f} = \frac{a_f^{q+1}}{q+1} = A\Delta\sigma_1^m N_{f_1} \qquad \text{(A3)}$$

So: $$N_{f_1} = \frac{a_f^{q+1} - a_0^{q+1}}{(q+1)A\Delta\sigma_1^m} \qquad \text{(A4)}$$

And similarly: $$N_{f_{21}} = \frac{a_f^{q+1} - a_0^{q+1}}{(q+1)A\Delta\sigma_{21}^m} \qquad \text{(A5)}$$

Now consider only n cycles are applied at the first stress level, so that the crack travels from a_0 to a_1. So: $$\frac{a_1^q - a_0^q}{q+1} = A\Delta\sigma_1^m n_1 \qquad \text{(A6)}$$

Therefore: $$n_1 = \frac{a_1^q - a_0^q}{(q+1)A\Delta\sigma_1^m} \qquad \text{(A7)}$$

Now consider the final n_2 cycles are applied at $\Delta\sigma_2$ as the crack travels from a_1 to a_2 (= a_f). Then:

$$\frac{a_f^q - a_1^q}{q+1} = A\Delta\sigma_2^m n_2 \qquad \text{(A8)}$$

So:

$$n_2 = \frac{a_f^q - a_1^q}{(q+1)A\Delta\sigma_2^m} \qquad \text{(A8)}$$

Hence:

$$\frac{n_1}{N_{f_1}} + \frac{n_2}{N_{f_2}} = \left(\frac{a_1^q - a_0^q}{B\Delta\sigma_1^m} \bullet \frac{B\Delta\sigma_1^m}{a_f^q - a_0^q}\right) + \frac{a_f^q - a_1^q}{a_f^q - a_0^q} \qquad \text{(A9)}$$

Where B=A(q+1), a constant. Other similar terms cancel out.

Hence:

$$\left(\frac{n_1}{N_{f_1}}\right) + \left(\frac{n_2}{N_{f_2}}\right) = \frac{a_1^q - a_0^q + a_f^q - a_1^q}{a_f^q - a_0^q} \qquad \text{(A10)}$$

$$\left(\frac{n_1}{N_{f_1}}\right) + \left(\frac{n_2}{N_{f_2}}\right) = \frac{a_f^q - a_0^q}{a_f^q - a_0^q} = 1 \qquad \text{(A11)}$$

References

1 Albert, W.A.J. (1838) Uber treibseile am harz. In: Archive fiir Mineralogie, Geognosie, Bergbau und Huttenkunde, Vol. 10, pp. 215-234.

2 Poncelet, J.V. (1839) Introduction a la mecanique industrielle. In: Physique ou Experimental Paris, pp. 317-318.

3 Rankine, W.J.M. (1843) On the causes of unexpected breakage of the journals of railway axles and the means of preventing such accidents by observing the law of continuity in their construction. Proceedings of the Institute of Civil Engineers 2, 105-108.

4 Wohler, A. (1867) Versuche liber die Festigkeit der Eisenbahnwagenachsen (English summary) Engineering 4,160-1.

5 Fairbairn, W. (1864) Experiments to determine the effect of impact, vibratory action, and long continued changes of load on wrought iron girders. Philosophical Transactions of the Royal Society, London 154, 311.

6 Gerber, H. (1874) Bestimmung der zuliissigen spannungen in eisen-konstructionen. Zeitschrift des Bayerischen Architekten und Ingenieur-Vereins 6, 101-110.

7 Goodman, J. (1899) Mechanics Applied to Engineering, Longmans Green, London.

8 Bauschinger, J. (1886) Ueber die Veranderungen der Elastizitatsgrenze und der Festigkeit des Eisens und Stahls Durch Strecken, Quetschen, Erwa'rmen, Abkiihlen und Durch Oftmals Wiederholte Belastung. Mitt: Mech-Tech Lab., XIII Munchen.

9 Ewing, J.A. and Rosenhain, W. (1900) Experiments in micro-metallurgy:-effects of strain. Preliminary notice. Philosophical Transactions of the Royal Society, London A199, 85-90.

10 Ewing, J.A. and Humfrey, J.C. (1903) The fracture of metals under rapid alterations of stress. Philosophical Transactions of the Royal Society, London A200, 241-250.

11 Basquin, O.H. (1910) The exponential law of endurance tests. Proceedings of the American Society for Testing and Materials 10, 625-630.

12 Palmgren, A. (1924) Die Lebensdauer von Kugellagern. Zeitschrift des Vereins Deutscher Ingenieure 68, 339-341.

13 Miner, M.A. (1945) Cumulative damage in fatigue. Journal of Applied Mechanics 12, 159-164.

14 Langer, B.F. (1937) Fatigue failure from stress cycles of varying amplitude. Journal of Applied Mechanics 59, 160-162.

15 Neuber, H. (1946) Theory of Notch Stresses: Principle for Exact Stress Calculations, Edwards, Ann Arbor, MI.

16 Zappfe, C.A. and Worden, C.O. (1951) Fractographic registrations of fatigue. Transactions of the American Society for Metals 43, 958-969.

17 Coffin, L.F. (1954) A study of the effects of cyclic thermal stresses on a ductile metal. Transactions of the American Society of Mechanical Engineers 76, 931-950.

18 Manson, S.S. (1954) Behaviour of Materials Under Conditions of Thermal Stress. National Advisory Commission on Aeronautics: Report 1170, Lewis Flight Propulsion Laboratory, Cleveland.

19 Suresh, S. (1998) Fatigue of Materials, Cambridge University Press, UK.

20 American Society for Testing and Materials (1974) STP 566 Handbook of Fatigue Testing, ASTM, USA.

21 Irwin, G.R. (1957) Analysis of Stresses and Strains Near the End of a Crack Traversing a Plate. Journal of Applied Mechanics 24, 361-364.

22 Forsyth, P.J.E. and Ryder, D.A. (1960) Fatigue Fracture. Aircraft Engineering 32,96-99.

23 Pans, P.C., Gomez, M.P. and Anderson, W.P. (1961) A Rational Analytic Theory of Fatigue. The Trend in Engineering 13, 9-14.

24 Paris, P.C. (1998) Fracture mechanics and fatigue: a historical perspective. Fatigue and Fracture of Engineering Materials and Structures 21, 535-540.

25 Elber, W. (1970) Fatigue Crack Closure under Cyclic Tension. Engineering Fracture Mechanics 2, 37-45.

26 Ritchie, R.O., Suresh, S. and Moss, C.M. (1980) Near-threshold fatigue crack growth in 2.25Cr-lMo pressure vessel steel in air and hydrogen. Journal of Engineering Materials and Technology 102, 293-299.

27 Suresh, S., Zamiski, G.F. and Ritchie, R.O. (1981) Oxide-induced crack closure: an explanation for near-threshold corrosion fatigue crack growth behaviour. Metallurgical Transactions 12A, 1435-1443.

28 Suresh, S. and Ritchie, R.O. (1984) Near-threshold fatigue crack propagation: a perspective on the role of crack closure. In: Fatigue Crack Growth Threshold Concepts (Edited by D.L. Davidson and S. Suresh), Warrendale, pp. 227-261, The Metallurgical Society of the American Institute of Mining, Mineral and Petroleum Engineers.

29 Shin, C.S. and Hsu, S.H., (1993) On the Mechanisms and Behaviour of Overload Retardation in AISI 304 Stainless Steel. Int. J. Fatigue. 15, 181-192.

30 Damri, D. and Knott, J.F. (1993) Fracture modes encountered following the application of a major tensile overload cycle. International Journal of Fatigue 15, 53-60.

31 Suresh, S. (1983) Micromechanisms of fatigue crack growth retardation following overloads. Engineering Fracture Mechanics 18, 577-593.

32 Hu, X.Z. and Mai, Y.W. (1992) A General Method for Determination of Crack-Interface Bridging Stresses. J. Mater. Sci. 27, 3502-3510.

33 Miller, KJ. (1999) Overview, Mixed mode crack behaviour. ASTM STP 1359, vii-ix.

34 Miller, K.J., Brown, M.W., Yates, J.R. (1999) Some observations on mixed-mode fatigue behaviour of polycrystalline metals. ASTM STP 1359, 229-257.

35 Forsyth, P.I.E. (1962) A two stage process of fatigue crack growth. Proceedings of Cranfie Id Symposium, Her Majesty's Stationery Office, London, 76-94.

36 Zappfe, C.A., Worden, C.O. (1951) Fractographic registrations of fatigue. Trans. of the American Society of Metals 43, 958-969.

37 Laird, C. (1967) The influence of metallurgical structure on the mechanisms of fatigue crack propagation, ASTM STP 415, 131-168.

38 Laird, C. (1979) Mechansims and theories of fatigue. In: Fatigue and Micro structure, American Society for Metals, OH, 149-203.

39 Lankford, J. and Davidson, D.L. (1983) Fatigue crack micromechanisms in ingot and powder metallurgy 7XXX aluminium alloys in air and vacuum. Acta Metallurgica, 31, 1273-1284.

40 Vasudeven, A.K., Sadananda, K., Louat, N. (1994) A review of crack closure, fatigue crack threshold and related phenomena. Mater. Sci. Engng. A188, 1-22.

41 McEvily, A.J., Ritchie, R.O. (1998) Crack closure and the fatigue-crack propagation threshold as a function of load ratio. Fatigue Fract. Engng. Mater. Struct. 21,847-855.

42 Atkins, A.G. and Mai, Y.W. (1988) Elastic and plastic fracture, John Wiley & Sons, UK.

43 Miller, K.J. and Zachariah, K.P. (1977) Cumulative damage laws for fatigue crack initiation and stage 1 propagation *Fat. Frac. Engng. Mater. Struc.* **12**, 262-285.

44 Chaboche, J.L, and Lesne, P.M. (1988) A non-linear continuous fatigue damage model. *Fat. Frac. Engng. Mater. Struc.* **11**, 1-17.

45 Chaboche, J.L., Kaczmarek, H. and Raine, P. (1981) Hardening and fatigue damage interaction in 316L stainless steel. *La Rech. Aérospatiale* (English Edition) No. 1980-3, 35-55.

46 Bolotin, V.W. (1989) Prediction of service life for machines and structures, ASME Press, New York.

47 Broek, D. (1985) Elementary Engineering Fracture Mechanics, Nijhoff, Netherlands.

48 Elber, W. (1970) Fatigue crack closure under cyclic tension. *Engng. Fract. Mech.* 2,37-45.

49 Hertzberg, R.W. (1989) Deformation and fracture mechanics of engineering materials. John Wiley and Sons, USA.

50 Suresh, S. and Ritchie, R.O. (1984) Propagation of short fatigue cracks. Int. Metall. Rev. 29, 445-476.

51 Shin, C.S. and Cai, C.Q. (2000) A model for evaluating the effect of fatigue crack repair by the infiltration method. *Fat. Frac. Engng. Mat. Struc.* **23**, 835.

52 Schijve, J. (1960) Fatigue crack propagation in light alloy sheet materials and structures. NRL Report MP 195. National Aeronautical and Astronautical Research Institute, Amsterdam.

53 Von Euw, E.F.J., Hertzberg, R.W., Roberts, R. (1972) Delay effects in fatigue crack propagation. ASTM STP 513, 230-259.

54 Ellyin, F., Wu, J. (1999) A numerical investigation on the effect of an overload on fatigue crack opening and closure behaviour. Fatigue Fract. Engng. Mater. Struct. 22, 835-847.

55 Carlson, R.L., Kardornateas, G.A., Bates, P.R. (1991) The effects of overloads in fatigue crack growth. Int. J. Fatigue 13, 453-460.

56 Kumar, R. (1992) Prediction of delay cycles due to instant of single overload cycles. Engng. Fract. Mech. 42, 563-571.

57 Tsukuda, H., Ogiyama, H. and Shiraishi, T. (1996) Transient fatigue crack growth behaviour following single overloads at high stress ratios. Fatigue Fract. Enging. Mater. Struct. 19, 879-891.

58 Craig, D., Kujawski, D., Ellyin, F. (1995) An experimental technique to study the behaviour of small corner cracks. Int. J. Fatigue 17, 253-259.

59 Skorupa, M. (1998) Load interaction effects during fatigue crack growth under variable amplitude loading - a literature review. Part I: Empirical trends. Fatigue Fract. Engng Mater. Struct. 21, 987-1006.

60 Skorupa, M. (1999) Load interaction effects during fatigue crack growth under variable amplitude loading - a literature review. Part II: Qualitative interpretation. Fatigue Fract. Engng Mater. Struct. 22, 905-926.

61 Ellyin, F. and Wu, J. (1999) A numerical investigation on the effect of an overload on fatigue crack opening and closure behaviour. *Fat. Frac. Engng. Mats. Struc.* **22**, 835..

62 Christensen, R.H. (1959) Fatigue crack, fatigue damage and their detection. In: Metal Fatigue, McGraw-Hill, New York.

63 Fleck, N.A. (1985) Influence of stress state on crack growth retardation. ASTM STP924, 157-183.

64 Hopper, T.H., Yu, M.T. (1985) The effect of overloads on threshold and crack closure. Int. J. Fatigue 3, 159-164.

65 Davidson, D.L. (1988) Determination of the local driving force for fatigue crack growth under variable amplitude loading. In: Fatigue crack growth under variable amplitude loading, Elsevier, London, 1-11.

66 Schijve, J., Broek, D. (1962) The result of a test programme based on a gust spectrum with variable amplitude loading. Aircraft Engineering 34, 314-316.

67 Jones, R.E., (1973) Fatigue crack growth retardation after single cycle peak overload in Ti-6Al-4V titanium alloy. Engng Fract. Mech. 5, 585-604.

68 Knott, J.F., Pickard, A.C. (1977) Effects of overloads on fatigue crack propagation: aluminium alloys. Mater. Sci. Engng 11, 399-404.

69 Rice, J.R. (1968) A path independent integral and the approximate analysis of strain concentrations by notches and crack. *J. Applied Mech* **35**, 379-86

70 Tomkins, B. (1968) Fatigue crack propagation – an analysis. *Phil. Mag*. **18**, 1041-1066.

71 ASTM (1991) £399-90, ASTM, USA.

72 Hu, X.Z. (1992) Influence of crack tip shielding on fatigue crack growth in ceramic materials. In: Proc. of the Inter. Ceramic Conf. (AUSTCERAM 92) (Edited by M.J. Bannister), Melbourne, Vol. 2, pp. 870-875.

73 Shuter, D.M. and Geary, W. (1996) Some aspects of fatigue crack retardation behaviour following tensile overloads in a structural steel. Fatigue Fract. Engng. Mater. Struct. 19, 185-199.

74 Ward-Close, C.M., Blohm, A.F. and Ritchie, R.O. (1989) Mechanisms associated with transient fatigue growth under variable-amplitude loading: an experimental and numerical study. Engng. Fract. Mech. 32, 613-638.

75 Dauskardt, R.H., Dalgleish, B.J., Yao, D., Ritchie, R.O. and Becher, P.F. (1993) Cyclic fatigue-crack propagation in a silicon carbide whisker-reinforced alumina composite: role of load ratio. /. Mater. Sci. 28, 3258-3266.

76 Dauskardt, R.H., Ritchie, R.O. and Cox, I.N. (1993) Fatigue of advanced materials: Part I. Adv. Mater. Processes 7, 26-30.

77 Ritchie, R.O. (1988) Mechanisms of fatigue crack propagation in metals, ceramics and composites: role of crack tip shielding. Mater. Sci. Engng A103, 15-28.

78 Shang, J.K., Tzou, J-L. and Ritchie, R.O. (1987) Role of crack tip shielding in the initiation and growth of long and small fatigue cracks in composite microstructures. Metall. Trans. ISA, 1613-1626.

79 Hou, C.Y. and Charng, J-J. (1996) Estimation of plasticity-induced crack closure in a pre-existing plastic zone. Int. J. Fatigue 18, 463-474.

80 Skorupa, M., Schijve, J., Skorupa. A., Machniewicz, T. (1999) Fatigue crack growth in a structural steel under single and multiple periodic overload cycles. Fatigue Fract. Engng Mater. Struct. 22, 879-887.

81 Wheeler, O.E. (1972) Spectrum loading and crack growth. J. Bas. Engng 94, 181-186.

82 Wheatley, G., Estrin, Y., Hu, X.Z. and Brèchet, Y. (1998) Effect of Low Cycle Fatigue on Subsequent High Cycle Fatigue Eife of 316L Stainless Steel. Mater. Sci. Engng A 254, 315-316.

83 Uemura, T. (1998) A fatigue life estimation of specimens excessively prestrained in tension. Fatigue Fract. Engng Mater. Struct. 21, 151-158.

84 Ding J., Huang H., McCormick PG., Street R. (1995) Magnetic properties of martensite-austenite mixtures in mechanically milled 304 stainless steel. JMMM 139, 109-114.

85 Dougherty, J.D., et al. (1997) Fatigue crack propagation and closure behaviour of modified 1070 steel: experimental results. Engng. Frac. Mech. 56,167-187.

~Fin~